

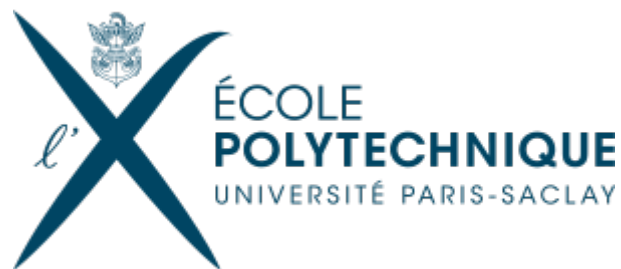
The Kitaev Model(s):  
Majorana Fermions and Quantum  
Computation

by  
**Fan Yang**

*M1 High Energy Physics*

Supervisor:

PROF. KARYN LE HUR



# Contents

<b>Introduction</b>	<b>1</b>
<b>1 Transverse Field Ising Model</b>	<b>4</b>
1.1 Jordan-Wigner Transformation . . . . .	4
1.2 Ground State . . . . .	5
1.2.1 Fermionic ground state . . . . .	6
1.2.2 BCS ground state . . . . .	7
1.3 Exact Spectrum . . . . .	7
1.4 Majorana operators . . . . .	8
1.5 Mapping of the quantum model in $d$ -dimensions to the classical model in $(d + 1)$ -dimensions . . . . .	10
<b>2 Single Spin Chain</b>	<b>11</b>
2.1 Eigenspectra . . . . .	13
2.2 Majorana chain representation . . . . .	14
2.3 Critical phenomena . . . . .	15
2.4 Spin duality transformation . . . . .	16
2.5 String order parameter . . . . .	17
2.6 Local Kitaev representation . . . . .	18
2.7 Correlation function . . . . .	19
2.8 Unpaired Majorana modes . . . . .	19
2.9 Perturbation theory study . . . . .	20
<b>3 Two-leg Spin Ladder</b>	<b>21</b>
3.1 Majorana picture . . . . .	21
3.1.1 String representation . . . . .	21
3.1.2 2D Kitaev representation . . . . .	23
3.2 $\mathbb{Z}_2$ gauge theories and generalised ladders . . . . .	24
3.3 Phase diagram with $J_4$ . . . . .	25
3.3.1 Free fermion model . . . . .	25
3.3.2 $J_4$ ladder . . . . .	26
3.3.3 $J_4 = 0$ . . . . .	28
3.3.4 $J_4 = J_3$ . . . . .	28
<b>Conclusion</b>	<b>29</b>

# Introduction

Since it was first hypothesized by Ettore Majorana in 1937, Majorana particle has sparked growing interests in both the fields of high energy physics and condensed matter physics. By definition, Majorana particle is a fermion that acts as its own antiparticle and thus uncharged. If we define a set of creation and annihilation operators  $\gamma_j^\dagger$  and  $\gamma_j$  of quantum state  $j$ , Majorana fermion satisfies

$$\gamma_j^\dagger = \gamma_j,$$

while for Dirac fermion, they are distinct.

In the realm of high energy physics, nearly all elementary fermions fall into the category of Dirac fermions, obtaining gauge charges in the Standard Model. One exception is the right-handed sterile neutrino. Predicted by the well-known seesaw mechanism [1], if we treat it as Majorana particle at low energy, the smallness of observed neutrino mass becomes natural after electroweak symmetry breaking. In addition, Majorana particle is also one promising candidate for dark matter in the universe [2]. However, experiments are still underway to search for such exotic Majorana particles. Neutrinoless double beta decay [3] and the production of lepton pairs with same charges at LHC [4], might produce encouraging evidence in the near future.

In condensed-matter systems, Majoranas emerge from microscopic models on a lattice which describe collective behaviours of atoms and the interactions with environment. They are more clean in materials than in accelerators, and make it easier for scientists to manipulate. So far, there are two classes of materials giving birth to Majoranas: topological superconductors and topological insulators.

For the first class, in 2000, N. Read and D. Green built Majorana fermions from a 2D  $p_x + ip_y$  superconductor, the mass of which would change the sign in the transition between weak- and strong-coupling Bardeen-Cooper-Schrieffer (BCS) paired states [5]. One year later, A. Kitaev predicted Majorana fermions should appear as stable edge states of a 1D superconducting  $p_x$ -wave wire and shed light on their potential role as a building block, namely the qubits, for a topological quantum computer [6]. More recently, theoretical observation has pointed to the existence of Majoranas in topological insulators [7] and superconducting graphene [8, 9]. For experimental detection, it was shown that the combination of spin-orbit coupling with a Zeeman field or strong interactions may lead to the formation of Majorana particles [10, 11]. Yet positive experimental results have not come out until 2012 when a neutral Majorana was observed in indium antimonide semiconductor nanowires connected to a gold and a superconductor at each end [12]. When exposed to strong magnetic field, the peak of electrical conductance at zero voltage supported Majorana bound states. However, it could not exclude the possibility of Kondo effect or disorder [13]. In 2014, stronger evidence was given by applying low-temperature scanning tunnelling microscope. It allowed to spatially resolve zero-bias peak features and demonstrated that Majoranas were localized at the boundary of iron atomic chains on the surface of superconducting lead [14].

We can briefly review how Majoranas arise from the BCS Hamiltonian using mean field theory [15, 16]. Written in the matrix form with the fermionic basis,

$$H_{\text{BCS}} = \sum_k \begin{pmatrix} f_k^\dagger & f_{-k} \end{pmatrix} \begin{pmatrix} T_k & \Delta_k \\ \Delta_k^* & -T_{-k} \end{pmatrix} \begin{pmatrix} f_k \\ f_{-k}^\dagger \end{pmatrix}, \quad (1)$$

$T_k$  represents the hopping term, and  $\Delta_k$  the pairing term. After diagonalization of the Hamiltonian, we can find the band structure with a superconducting gap (see Fig. 1). It takes finite energy to create a pair of quasi-particle and quasi-hole. On the Fermi level, we get Majorana zero modes (MZM) where the particle and hole coincide with each other:

$$\epsilon_k - \mu = 0, \quad k = k_F.$$

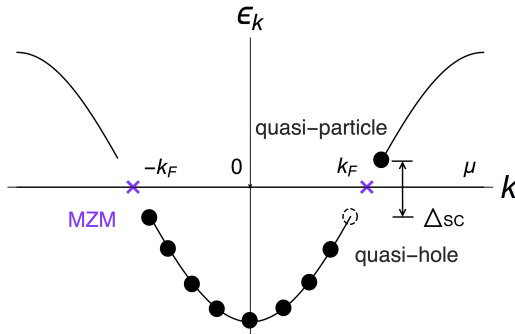


Figure 1: Band structure of the BCS Hamiltonian.

Here  $\mu$  represents the chemical potential of the system. We further denote the eigenvector as  $\gamma_k$  and it must satisfy:

$$\gamma_k = u_k f_k + v_k f_{-k}^\dagger, \quad \gamma_k^\dagger = \gamma_k, \quad u_k = v_k^*.$$

Now if we exchange the particle and hole by  $\sigma^1$  Pauli matrix, due to their opposite signs of energies, we arrive at

$$\begin{aligned} \sigma^1 H_{\text{BCS}} \sigma^1 &= -H_{\text{BCS}}^*, \\ \begin{pmatrix} 0 & 1 \\ 1 & 0 \end{pmatrix} \begin{pmatrix} T_k & \Delta_k \\ \Delta_k^* & -T_{-k} \end{pmatrix} \begin{pmatrix} 0 & 1 \\ 1 & 0 \end{pmatrix} &= \begin{pmatrix} -T_{-k} & \Delta_k^* \\ \Delta_k & T_k \end{pmatrix} = \begin{pmatrix} -T_{-k} & -\Delta_{-k}^* \\ -\Delta_{-k} & T_k \end{pmatrix}, \\ \Delta_k &= -\Delta_{-k}. \end{aligned}$$

So to hold Majorana particles, the pairing term should have odd parity, which corresponds to the  $p$ -wave superconductors. In real life, as they are not so common, they have another name “topological superconductors”.

Further, we notice from (1), the superconducting gap  $\Delta_k$  and  $\Delta_k^*$  are associated with bosonic pairing operators  $f_k^\dagger f_{-k}^\dagger$  and  $f_{-k} f_k$ . At low temperatures, due to Bose-Einstein condensation, there are no back-scattered electrons. It gives rise to the zero resistance of superconductors below  $T_C$ . For the second class topological insulators, the mechanism is quite different. It starts from an insulating phase to build effective lattice models where particles are localized at each site. A. Kitaev first came up with an exactly solvable model on honeycomb lattices with four Majoranas per site in two dimensions [17].

For real quantum materials, we mainly focus on the Heisenberg-Kitaev (HK) model:

$$H_{\text{HK}} = \sum_{\langle ij \rangle \in \alpha} (J \mathbf{S}_i \cdot \mathbf{S}_j + K S_i^\alpha S_j^\alpha), \quad \alpha = x, y, z, \quad (2)$$

where  $J$  denotes the Heisenberg coupling constant and  $K$  represents the Kitaev exchange on  $\langle ij \rangle$  links from three different directions. The phase diagram in Fig. 2 can be used to study the stability of Kitaev spin liquid and its neighbouring phases [18]. Similar to neutrino mixing angles, here  $\phi$  is introduced to parametrize the model:  $J = \cos \phi, K = \sin \phi$ . We shall see later in Sec. 2.9, Heisenberg coupling will destroy free Majorana particles. In correlated materials like honeycomb iridium oxides, the difficulty lies in the fact usually Heisenberg interactions can not be neglected and in most cases, the system exhibits a zigzag ordering. While the featureless Majorana bound states are rather difficult both for the formation and identification, encouragingly, excited states of Majorana fermions have just been reported in the honeycomb magnet  $\alpha$ -RuCl<sub>3</sub> [19]. On the other hand, in ultracold atom experiments, the mixing angle can be carefully tuned. When  $|K| \gg |J|, \phi \sim \pi/2, 3\pi/2$ , we are expected to build pure Kitaev optical lattices and reach two spin liquid points in Fig. 2. Real efforts have been put into the field of quantum engineering [20].

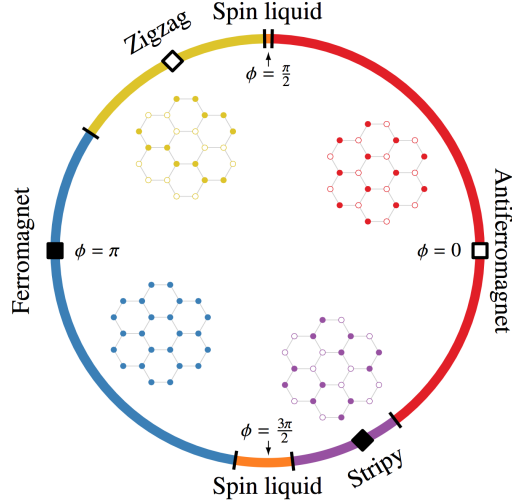


Figure 2: Phase diagram of the Heisenberg-Kitaev model [18].

In this report, our goal is to explore low-dimensional analogues of BCS form (1). We are going to construct Majorana fermions in the spin-1/2 models which are insulating in one and two dimensions. Our general approach will start from the Jordan-Wigner transformation [21], which maps spin operators to fermionic operators  $a$  and  $a^\dagger$ . We can look at the simplest single-spin case:

$$\sigma^+ = a, \quad \sigma^- = a^\dagger, \quad \sigma^z = 1 - 2a^\dagger a = \begin{cases} 1, & |\uparrow\rangle \\ -1, & |\downarrow\rangle \end{cases}, \quad \{a, a^\dagger\} = 1,$$

where the spin-down state is full and the spin-up state is empty. It is easy to see that the spin operators then fulfil the anti-commutation relations:

$$\begin{aligned} \sigma^x &= \sigma^+ + \sigma^-, & \sigma^y &= \frac{1}{i} (\sigma^+ - \sigma^-), \\ [\sigma^x, \sigma^y] &= \frac{1}{i} [a + a^\dagger, a - a^\dagger] = 2i(1 - 2a^\dagger a) = 2i\sigma^z. \end{aligned}$$

However, for multi-spin systems it becomes more complicated. To do the exact mapping, we have to introduce strings into Jordan-Wigner transformation (see Sec. 1.1). For the next step, we can construct Majorana particles from these fermionic operators. With respect to single-spin system, in total we have two Majoranas  $c$  and  $d$ :

$$c = a + a^\dagger, \quad d = i(a^\dagger - a).$$

If both of them are free, the eigenstates  $|0\rangle$  and  $|1\rangle$  of one qubit can be further built:

$$g^\dagger = \frac{1}{2}(c + id), \quad g = \frac{1}{2}(c - id), \quad g^\dagger|0\rangle = |1\rangle, \quad g|1\rangle = |0\rangle.$$

Exchanging  $c$  and  $d$  will always give an extra factor  $(-i)$ , which is the characteristic of Majorana braiding (see Fig. 3).

Based on the above discussion, in Sec. 1, we summarize a well-known exactly solvable model exhibiting Majoranas, the quantum Ising chain which is linked with BCS ground states. In Sec. 2 and 3, magnetic analogues of the 2D Kitaev model are probed. We will also take advantage of emergent Majorana fermions and build their connections to potential materials realization and quantum computation.

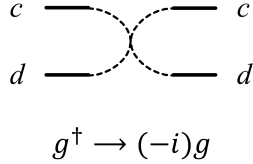


Figure 3: Braiding of two Majoranas.

## 1 Transverse Field Ising Model

In this section, we aim to discuss, as an introduction, a model with magnetic spins showing low-energy Hamiltonian of the form (1). Starting from the quantum Ising chain with interaction Hamiltonian:

$$H_I = -J \sum_i (g \hat{\sigma}_i^z + \hat{\sigma}_i^x \hat{\sigma}_{i+1}^x), \quad (3)$$

where  $J > 0$  is an exchange constant and  $g > 0$  is a dimensionless coupling, we first introduce Jordan-Wigner transformation to obtain a similar form as the BCS Hamiltonian. It enables us to discuss the ground states under different limits of  $g$  and solve the exact spectrum. We will see quantum phase transition at the critical point  $g_C = 1$  between distinct magnetic configurations. When we move into the Majorana picture, they correspond to different couplings of Majorana particles. At the end of this section, we will perform the mapping from the quantum model in one dimension to the 2D classical Ising model. It will deepen our understanding of the critical phenomena of quantum spin chain in Sec. 2.

### 1.1 Jordan-Wigner Transformation

Jordan-Wigner transformation has a historical significance in modern physics. In 1925, Dirac introduced the creation and annihilation operators  $a^\dagger$  and  $a$  to reinterpret the fundamental equations of quantum mechanics into the matrix formulation [22]. Only three years later, P. Jordan and EP Wigner constructed a transformation from spin operators to fermionic creation and annihilation operators  $a^\dagger$  and  $a$  [21]. However, it had to wait until 1940 when T. Holstein and H. Primakoff found its first application in atomic magnets [23]. In 1957, the BCS ground state was built and it showed a close connection to the spin liquid phase in magnets [15]. In 1983, based on Holstein-Primakoff boson representation, FDM. Haldane solved the 1D Heisenberg antiferromagnetic chain [24]. Nearly twenty years later, a more general spin-fermion transformation was developed, leading to Majorana representation and the first 2D spin-1/2 model was exactly solved by A. Kitaev [17].

Going back to the quantum Ising chain, we introduce Jordan-Wigner transformation in the following form:

$$\sigma_j^+ = a_j e^{i\pi \sum_{i<j} \tilde{Q}_i}, \quad \sigma_j^- = a_j^\dagger e^{i\pi \sum_{i<j} \tilde{Q}_i} \quad \tilde{Q}_i = a_i^\dagger a_i, \quad (4)$$

where  $a_i^\dagger$  and  $a_i$  are fermionic creation and annihilation operators which satisfy

$$\{a_i, a_j^\dagger\} = \delta_{ij}, \quad \{a_i, a_j\} = \{a_i^\dagger, a_j^\dagger\} = 0.$$

It maps the Hilbert space of a system with spin 1/2 per site into that of spinless fermions hopping between sites. And we denote the spin-up state as empty and spin-down state as occupied.

$$\begin{aligned} \sigma_j^x &= \sigma_j^+ + \sigma_j^- = (a_j^\dagger + a_j) e^{i\pi \sum_{i<j} a_i^\dagger a_i}, \\ \sigma_j^y &= \frac{1}{i} (\sigma_j^+ - \sigma_j^-) = i(a_j^\dagger - a_j) e^{i\pi \sum_{i<j} a_i^\dagger a_i}, \end{aligned} \quad (5)$$

$$\sigma_j^z = -i\sigma_j^x \sigma_j^y = (a_j^\dagger + a_j)(a_j^\dagger - a_j) = 1 - 2a_j^\dagger a_j = e^{i\pi a_j^\dagger a_j} = \begin{cases} 1, & |\uparrow\rangle; \\ -1, & |\downarrow\rangle. \end{cases}$$

We notice the quantization axis is not chosen as the normal Néel order. It implies when  $g \rightarrow 0$ , the ground state with spins oriented along  $x$  axis  $|\leftarrow\leftarrow\leftarrow\rightarrow\rightarrow\rangle$ , will result in  $\langle\sigma_j^z\rangle = 0$ ,  $\langle a_j^\dagger a_j \rangle = 1/2$ . We always get a half-filled band.

It can be verified that if the anti-commutation relations hold for  $a_i$ ,  $a_i^\dagger$ , the spin operators are consistent with the following commutation relations, and vice versa:

$$[\hat{\sigma}_i^+, \hat{\sigma}_j^-] = \delta_{ij} \hat{\sigma}_i^z, \quad [\hat{\sigma}_i^z, \hat{\sigma}_j^\pm] = \pm 2\delta_{ij} \hat{\sigma}_i^\pm.$$

Then we obtain a quadratic Hamiltonian in free Fermionic operators,

$$H_I = -J \sum_i \left( a_i^\dagger a_{i+1}^\dagger + a_i^\dagger a_{i+1} + a_{i+1}^\dagger a_i + a_{i+1} a_i - 2g a_i^\dagger a_i + g \right). \quad (6)$$

The system is in a grand canonical ensemble with the chemical potential

$$\mu = \epsilon_F = -2Jg, \quad E_{GS} = \langle N \rangle \epsilon_F = \sum_i \mu \langle a_i^\dagger a_i \rangle.$$

## 1.2 Ground State

As  $H_I$  (6) is quadratic in Fermionic operators, we can diagonalize it in the momentum space:

$$a_i = \frac{1}{\sqrt{M}} \sum_k \langle x_i | k \rangle \langle k | a \rangle = \frac{1}{\sqrt{M}} \sum_k e^{ikx_i} a_k, \quad a_i^\dagger = \frac{1}{\sqrt{M}} \sum_k e^{-ikx_i} a_k^\dagger, \\ k = \frac{2\pi m}{l}, \quad m = -\frac{M}{2}, \dots, 0, \dots, \frac{M}{2} - 1,$$

where  $M$  is the number of sites,  $l$  is the lattice spacing and  $x_m = ml$ ,  $L = Ml$ .

$$H_I = J \sum_k \left( 2(g - \cos(kl)) a_k^\dagger a_k - g + i \sin(kl) (a_{-k}^\dagger a_k^\dagger + a_{-k} a_k) \right), \quad (7)$$

where  $b_k^\dagger = a_{-k}^\dagger a_k^\dagger$  and  $b_{-k} = a_{-k} a_k$  are bosonic operators  $[b_k, b_{k'}^\dagger] = \delta_{k,k'} - \delta_{k,-k'}$ . Hamiltonian (7) consists of two parts: the diagonal and the off-diagonal terms

$$H_0 = \sum_k 2J(g - \cos(kl)) a_k^\dagger a_k - Jg, \quad H_1 = \sum_k iJ \sin(kl) (a_{-k}^\dagger a_k^\dagger + a_{-k} a_k). \quad (8)$$

To keep the total particle number  $\hat{N} = \sum_k a_k^\dagger a_k$  conserved, we can enlarge the Hilbert space of  $H_0$  to twice of its original size,

$$H'_0 = 2H_0 = H_0 + H_{\text{equiv}}, \\ H_{\text{equiv}} = \sum_k 2J(g - \cos(-kl)) a_{-k}^\dagger a_{-k} - Jg, \\ H'_0 = \sum_k (-2J \cos(kl) - \mu) (a_k^\dagger a_k - a_{-k} a_{-k}^\dagger).$$

If we choose  $(a_k^\dagger, a_{-k})$  as our basis, in the matrix form

$$H'_0 = \sum_k \begin{pmatrix} a_k^\dagger & a_{-k} \end{pmatrix} \begin{pmatrix} -2J \cos(kl) - \mu & 0 \\ 0 & 2J \cos(kl) + \mu \end{pmatrix} \begin{pmatrix} a_k \\ a_{-k}^\dagger \end{pmatrix}, \quad (9)$$

$$H_1 = \sum_k \begin{pmatrix} a_k^\dagger & a_{-k} \end{pmatrix} \begin{pmatrix} 0 & -iJ \sin(kl) \\ iJ \sin(kl) & 0 \end{pmatrix} \begin{pmatrix} a_k \\ a_{-k}^\dagger \end{pmatrix}. \quad (10)$$

Here (9) and (10) share the same form with the BCS Hamiltonian (1):  $f_k = a_k$ ,  $f_{-k}^\dagger = a_{-k}^\dagger$ ,  $T_k = -2J \cos(kl) - \mu$ ,  $\Delta_k = -iJ \sin(kl)$ . The two diagonal elements give the energies to create one particle  $a_k^\dagger a_k$  and one hole  $a_{-k} a_{-k}^\dagger$ . They have opposite signs, corresponding to the positive energy of particles and negative energy of anti-particles. For off-diagonal terms,  $\Delta_k = -\Delta_{-k}$ . This odd parity shows the feature of  $p_x$ -wave superconductors.

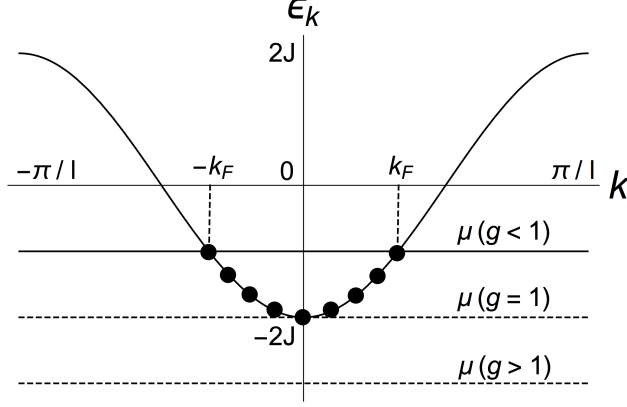


Figure 4: Band structure of  $H_0$ . ( $J > 0$ )

### 1.2.1 Fermionic ground state

First, we only consider the effect of  $H'_0$  on the band structure of particles.

$$H_0 = \sum_k \tilde{\epsilon}_k a_k^\dagger a_k, \quad \tilde{\epsilon}_k = -2J \cos(kl) - \mu = \epsilon_k - \mu,$$

where  $\epsilon_k$  is the energy of one particle at wave vector  $k$ . We fix  $\mu$  and get the fermi energy,  $\tilde{\epsilon}_{k_F} = -2J \cos(k_F l) - \mu = \epsilon_{k_F} - \mu = 0$ . It is clear that only when  $\mu = -2Jg > -2J, g < 1$ , the fermi level will cross the band (see Fig. 4). The system behaves like a metal. When  $g > 1$ , there is a gap between the fermi level and the bottom of the band. As it costs finite energy to add one particle from the vacuum, the system exhibits an insulating phase. When  $g = 1$ , the band becomes gapless.

Particles can only occupy states below  $\epsilon_F$ , we obtain the fermionic ground state:

$$|GS\rangle_0 = \prod_{|k| \leq k_F} a_k^\dagger |0\rangle = |k_n, \dots, k_1\rangle_{|k_i| \leq k_F}, \quad (11)$$

where  $|0\rangle$  is the vacuum state defined by  $a_k |0\rangle = 0, \forall k$ . Total mean number of particles of the system becomes

$$\langle N \rangle = \sum_i {}_0 \langle GS | a_i^\dagger a_i | GS \rangle_0 = \frac{Ml}{\pi} k_F.$$

The unit of  $\langle N \rangle$  being 1,  $k_F \sim \frac{1}{l}$  and  $\langle N \rangle \sim M$ , which is consistent with the fact

$$M \rightarrow \infty, \quad \frac{\langle (\delta N)^2 \rangle}{\langle N \rangle^2} = \frac{\langle N^2 \rangle - \langle N \rangle^2}{\langle N \rangle^2} \rightarrow \frac{1}{\langle N \rangle} \rightarrow 0.$$

If we assume  $\langle a_i^\dagger a_i \rangle = \langle a_j^\dagger a_j \rangle, i \neq j$  when  $M \rightarrow \infty$ , the mean number of particle per site becomes

$$\langle a_i^\dagger a_i \rangle = \frac{\langle N \rangle}{M} = \frac{l}{\pi} k_F = \begin{cases} (\arccos g) / \pi, & 0 < g < 1; \\ 0, & g \geq 1. \end{cases}$$

The band is unoccupied for  $g \geq 1$  and half-filled for  $g = 0$ .

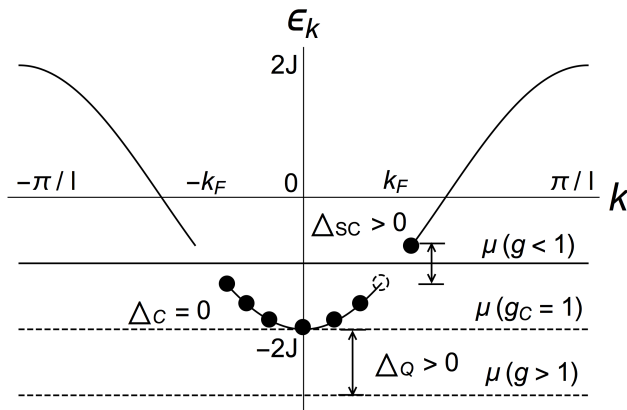


Figure 5: Effect of  $H_1$  on the band structure around the fermi level. ( $J > 0$ )

### 1.2.2 BCS ground state

Now we take  $H_1$  into account. On the fermi level,  $\frac{1}{2}H'_0 = H_0 = H_{\text{equiv}} = 0$ . In the total Hamiltonian, we only have the off-diagonal term (10) with eigenvalues:

$$H_1 = \begin{pmatrix} a_{k_F}^\dagger & a_{-k_F} \end{pmatrix} \begin{pmatrix} 0 & -iJ \sin(k_F l) \\ iJ \sin(k_F l) & 0 \end{pmatrix} \begin{pmatrix} a_{k_F} \\ a_{-k_F}^\dagger \end{pmatrix},$$

$$\begin{vmatrix} -\lambda & -iJ \sin(k_F l) \\ iJ \sin(k_F l) & -\lambda \end{vmatrix} = 0, \quad \lambda_{\pm} = \pm |J \sin(k_F l)|. \quad (12)$$

Considering different limits (see Fig. 5), when  $g \gg 1$ , the fermi level is well below the lowest band. The insulating band structure remains the same. To add one extra particle from the vacuum, it will still take finite energy which we call a charge gap  $\Delta_Q$ . When  $g = 1$ , the bottom of the band coincides with  $\epsilon_F$  ( $k_F = 0$ ). Thus  $\Delta_C = 2J |\sin(k_F l)| = 0$ , the system reveals a gapless mode. Whereas when  $g \rightarrow 0$ , it will open a gap  $\Delta_{SC} = 2J |\sin(k_F l)|$  around the fermi level, corresponding to the minimum excitation energy. As can be seen from (8),  $H_1$  always pairs particles with opposite momentums. So in this case, the system is in the superconducting phase with a gap in the energy spectrum. For the moment, we can tell from the gap evolution that there exists a quantum phase transition at  $g_C = 1$ .

We notice  $H'_0$  is invariant under the unitary transformation of the basis  $\tilde{\alpha} a_k + \tilde{\beta} a_{-k}^\dagger$ . As a result, the ground state is totally determined by the off-diagonal part  $H_1$ . In momentum space (7), it brings fermions with opposite momentums to form bosonic Cooper pairs  $b_k^\dagger = a_{-k}^\dagger a_k^\dagger$ . In the coordinate space (6), however, when  $g \rightarrow 0$ ,  $H_I$  pairs particles in the  $i$ th and  $(i+1)$ th sites. This point can also be reflected in the Majorana picture (see Fig. 6).

Based on above discussion, the ground state of the full Hamiltonian takes the BCS form without spin:

$$|GS\rangle = \prod_k \left( s_k + t_k a_k^\dagger a_{-k}^\dagger \right) |0\rangle, \quad (13)$$

where  $|s_k|^2 + |t_k|^2 = 1$  and  $|t_k|^2$  refers to the probability of the pair  $(k, -k)$  being occupied.

### 1.3 Exact Spectrum

Now we do a unitary Bogoliubov transformation from  $a_k, a_k^\dagger$  to a new set of fermionic operators  $\gamma_k, \gamma_k^\dagger$  so that the total number of free fermions  $\gamma$  is conserved and  $H_I$  is diagonalized.

$$\begin{aligned} \begin{pmatrix} \gamma_k \\ \gamma_{-k}^\dagger \end{pmatrix} &= U \begin{pmatrix} a_k \\ a_{-k}^\dagger \end{pmatrix} = \begin{pmatrix} u_k & -iv_k \\ -iv_k & u_k \end{pmatrix} \begin{pmatrix} a_k \\ a_{-k}^\dagger \end{pmatrix}, & UU^\dagger &= I, \\ \{\gamma_k, \gamma_{k'}^\dagger\} &= \delta_{k,k'}, & \{\gamma_k, \gamma_{k'}\} &= \{\gamma_k^\dagger, \gamma_{k'}^\dagger\} = 0, \end{aligned} \quad (14)$$

where  $u_k, v_k$  are real numbers and satisfy  $u_k^2 + v_k^2 = 1, u_k = u_{-k}, v_k = -v_{-k}$ .

Inserting (14) into (7), we have

$$H_I = \sum_k (A - C) \gamma_k^\dagger \gamma_k - C \gamma_{-k}^\dagger \gamma_{-k} + C - g + D \left( \gamma_k^\dagger \gamma_{-k}^\dagger + \gamma_k \gamma_{-k} \right)$$

where  $A = 2J(g - \cos(kb)), B = iJ \sin(kb), C = v_k^2 A + 2iu_k v_k B, D = (-u_k^2 + v_k^2)B + iu_k v_k A$ . The number of fermions should be conserved ( $D = 0$ ) and by introducing  $\theta_k$ , we get the constraint

$$u_k = \cos(\theta_k/2), \quad v_k = \sin(\theta_k/2), \quad \tan \theta_k = \frac{2B}{iA} = \frac{\sin(kl)}{g - \cos(kl)}.$$

Then  $H_I$  becomes diagonalized,

$$H_I = \sum_k \tilde{\epsilon}_k \left( \gamma_k^\dagger \gamma_k - \frac{1}{2} \right), \quad (15)$$

where  $\tilde{\epsilon}_k$  is the single-particle excitation energy:

$$\tilde{\epsilon}_k = \sqrt{A^2 - 4B^2} = 2J \sqrt{g^2 - 2g \cos(kl) + 1}, \quad \tilde{\epsilon}_k = \epsilon_k - \mu. \quad (16)$$

When  $k = k_F, -2J \cos(k_F l) = -2Jg, \tilde{\epsilon}_{k_F} = 2J |\sin(k_F l)| = \Delta_{SC}$ . By making an analogy with our former picture in (12), we see  $\tilde{\epsilon}_{k_F}$  is exactly the energy to add one quasiparticle above the superconducting gap.

Now we can examine the behaviors of  $\epsilon_k$  in the large and small  $g$  limits:

$$g \gg 1, \quad \epsilon_k = 2Jg \left( 1 - \frac{\cos(kl)}{g} + \frac{1}{4g^2} (1 - \cos(kl)) + \mathcal{O}\left(\frac{1}{g^3}\right) \right),$$

For the ground state, the spins are oriented in the same  $z$  direction  $|\uparrow\uparrow\uparrow\uparrow\uparrow\rangle$  and a paramagnetic mode dominates.

$$g \ll 1, \quad \epsilon_k = 2J (1 - g \cos(kl)) + \mathcal{O}(g^2),$$

There are domain walls between two ground states, like  $|\leftarrow\leftarrow\leftarrow\rightarrow\rightarrow\rightarrow\rangle$ .

In fact, the transverse field Ising model can be mapped into the spin-polarized 1-D superconductor (compared with equation (7)):

$$H_F = - \sum_i \left( w(a_i^\dagger a_{i+1}) + \Delta a_{i+1} a_i + \Delta^* a_{i+1}^\dagger a_i^\dagger \right) - \mu \sum_i \left( a_i^\dagger a_i - \frac{1}{2} \right),$$

when  $w = \Delta = \Delta^* = J, \mu = -2Jg$ . Here  $w$  stands for the hopping amplitude,  $\Delta$  represents the superconducting gap and  $\mu$  is the chemical potential.

## 1.4 Majorana operators

Alternatively, we can also transform this set of  $M$  Dirac fermions into a new set of  $2M$  Majorana fermions in Kitaev's approach [25]:

$$c_i = a_i + a_i^\dagger, \quad d_i = i(a_i^\dagger - a_i). \quad (17)$$

They are real and consistent with the anti-commutation relation:

$$c_i^\dagger = c_i, \quad d_i^\dagger = d_i, \quad \{c_i, c_j\} = \{d_i, d_j\} = 2\delta_{ij}.$$

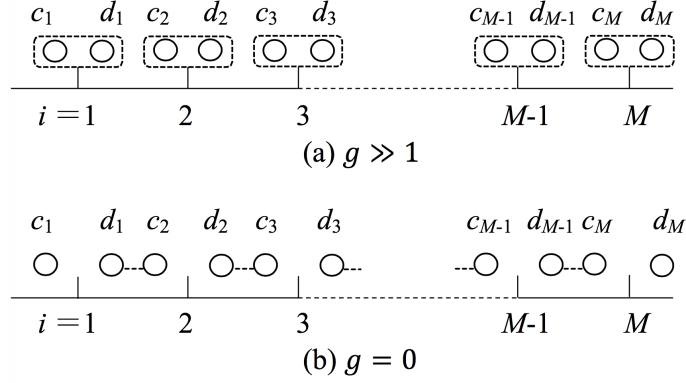


Figure 6: Majorana chain representation of the transverse field Ising model.

The interaction Hamiltonian (6) will be

$$H_I = iJ(g \sum_{i=1}^M c_i d_i + \sum_{i=1}^{M-1} d_i c_{i+1}). \quad (18)$$

When  $g \gg 1$ , we can ignore the interaction between  $d_i$  and  $c_{i+1}$  and obtain the pairs of Majoranas  $(c_i, d_i)$ . As shown in Fig. 6 (a), there is no free particle in the chain. When  $g = 0$ , we get two free Majorana modes  $c_1, d_M$  and the 2-fold ground state degeneracy could be represented in their tensor space  $c_1 \otimes d_M$ . See Fig. 6 (b).

We introduce new operators:

$$f^\dagger = \frac{1}{2}(c_1 + id_M), \quad f = \frac{1}{2}(c_1 - id_M). \quad (19)$$

In the language of quantum computation,  $f^\dagger$  and  $f$  are creation and annihilation operators for two eigenstates 1 and 0 of the qubit, which are pseudo-fermion states:

$$f^\dagger|0\rangle = |1\rangle, \quad f|1\rangle = |0\rangle.$$

To manipulate the state of one qubit, we need to exchange  $f^\dagger$  and  $f$ . From (19), this can be accomplished by the transformation  $id_M \leftrightarrow -id_M$ . Suppose at zero temperature, the spin chain has the configuration of  $|\rightarrow \rightarrow \dots \rightarrow\rangle$  and we associate it with the state  $f^\dagger$  (see Fig. 7 (a)). First we choose an arbitrary site  $j$  and add a small local magnetic field  $-h\hat{\sigma}_j^z$  ( $h > 0$ ) in favour of  $|\uparrow\rangle_j$ . It will not effect the physical ground state  $|\rightarrow \rightarrow \dots \rightarrow\rangle$  as  $h \rightarrow 0^+$ . Then we change the direction of the magnetic field  $h \rightarrow 0^-$  in Fig. 7 (b), which makes  $|\downarrow\rangle_j$  more favourable. Jordan-Wigner transformation (5) implies along the quantized  $x$ -axis

$$\hat{\sigma}_j^z = 1 - 2a_j^\dagger a_j = -ic_j d_j = \begin{cases} 1, & |\uparrow\rangle_j; \\ -1, & |\downarrow\rangle_j, \end{cases}$$

the product  $(-ic_j d_j)$  should change the sign. And we assume

$$id_j \rightarrow -id_j, \quad c_j \rightarrow c_j.$$

Meanwhile from (18), the original interaction Hamiltonian has a  $\mathbb{Z}_2$  symmetry reflected in the fermionic parity operator,

$$P_{\text{maj}} = \prod_{i=1}^M (-ic_i d_i), \quad [H_I, P_{\text{maj}}] = 0.$$

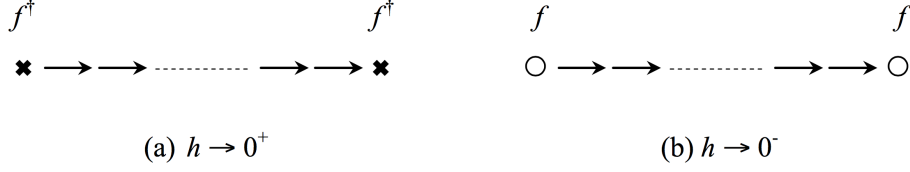


Figure 7: Exchange of qubits for 1D quantum Ising chain in the presence of small magnetic field along  $z$ -axis ( $-h\hat{\sigma}^z$ ). The sign of  $h$  changes over time.

The perturbative magnetic field  $-h\hat{\sigma}_j^z = hic_j d_j$  will not break this symmetry. To conserve parity, we have to do the transformation on all sites,

$$id_m \rightarrow -id_m, \quad c_m \rightarrow c_m, \quad m = 1, 2, \dots, M, \quad M \in \text{even}.$$

Total even number of sites will give a factor  $(-1)^M$ , leaving  $P_{\text{maj}}$  unchanged. Accordingly, the magnetic field has now been applied to every site. In particular,

$$c_1 \rightarrow c_1, \quad id_M \rightarrow -id_M, \quad f^\dagger \rightarrow f.$$

In experiments, however, one big challenge is for  $T > 0$ , the ground state is not pure with domain walls in between. Thus it becomes quite difficult to manipulate the qubit for the spin chain. The earliest real attempt has been made in [26].

## 1.5 Mapping of the quantum model in $d$ -dimensions to the classical model in $(d + 1)$ -dimensions

Quantum models in  $d$ -dimensions can be mapped to classical models in  $d + 1$  dimensions [27]. In our case taking  $d = 1$ , we are going to find a link between 1D quantum Ising model and 2D classical Ising model.

By rotating the spin axes 90 degrees around  $y$ -axis,  $\hat{\sigma}_j^z \rightarrow \hat{\sigma}_j^x, \hat{\sigma}_j^x \rightarrow -\hat{\sigma}_j^z$ , the quantum ferromagnetic Ising chain (3) can be written into the general form:

$$H_I = - \sum_j (Jg\sigma_j^x + J\sigma_j^z\sigma_{j+1}^z),$$

with the partition function  $Z = \text{Tr} \exp(-\beta_q H_I), \beta_q = \frac{1}{T_q}$ . If the quantum spin chain is parallel to  $x$ -axis, we can assume  $\beta_q$  represents the evolution along  $y$ -axis and set  $\beta_q = Ml$ . As  $T_q$  is finite,  $M \rightarrow \infty, l \rightarrow 0$ . The transfer matrices  $T_1, T_2$  can be introduced by the following approximation:

$$\begin{aligned} \exp\left(\sum_j Jgl\sigma_{j,k}^x + Jl\sigma_{j,k}^z\sigma_{j+1,k}^z\right) &\simeq \exp\left(\sum_j Jgl\sigma_{j,k}^x\right) \exp\left(\sum_j Jl\sigma_{j,k}^z\sigma_{j+1,k}^z\right) + \mathcal{O}(l^2). \\ Z &\simeq \text{Tr}(T_1 T_2)^M, \quad T_1 = \exp\left(\sum_j Jgl\sigma_{j,k}^x\right), \quad T_2 = \exp\left(\sum_j Jl\sigma_{j,k}^z\sigma_{j+1,k}^z\right). \end{aligned}$$

If we choose the eigenstates  $\{m_{j,k} = \pm 1\}$  of  $\sigma_{j,k}^z$  as the basis

$$Z = \sum_{\{m_{j,k}\}} \exp\left(\sum_{j,k} (Jlm_{j,k}m_{j+1,k} + Bm_{j,k}m_{j,k+1})\right), \quad (20)$$

where  $\tanh(gJl) = \exp(-2B)$ . The final mapping gives exactly 2D classical Ising model with different exchange constants in  $x$  and  $y$  directions.

Further, if we treat 2D classical Ising model by the mean field theory, the Hamiltonian will return to 1D case:

$$H_{cl} = -J \sum_{\langle i,j \rangle} s_i s_j, \quad (21)$$

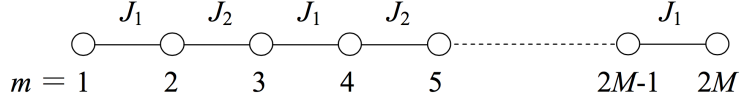


Figure 8: Single spin chain.

where each spin at site  $i$  takes the value  $\pm 1$ . The mean magnetization per site is given by  $m = (M_\uparrow - M_\downarrow)/M$ .  $\langle i, j \rangle$  represents the nearest pairs and  $M$  is the total number of sites. It can be shown that the free energy per site

$$f(T, m) = \frac{k_B}{2}(T - T_C)m^2 + \frac{k_B T}{12}m^4 - k_B T \log 2 + \mathcal{O}(m^4), \quad (22)$$

$$Z_{cl} = \exp\left(-\frac{1}{k_B T} \sum_j f(T, m)_j\right) \simeq \exp\left(-\sum_j \frac{T - T_C}{2T} m^2\right). \quad (23)$$

By comparison, in the mean-field approach, the partition function (20) becomes

$$Z = \sum_{\{m_{j,k}\}} \exp\left(\sum_{j,k} J l m^2\right), \quad J l \simeq B. \quad (24)$$

As a result, the coupling constants in (23) and (24) should be the same and around the classical critical temperature,

$$T \rightarrow T_C, \quad J l \simeq -\frac{T - T_C}{2T_C} \rightarrow 0.$$

We verify that the coupling constants in quantum models can be expressed as a function of the critical temperature  $(T - T_C)/T_C$  in classical models. Therefore, classical critical phenomena which take place at  $T_{cl} = T_C$  have a clear correspondence with the quantum phase transitions at  $T_q = 0$  when  $g \rightarrow g_C$ .

In the end, we can also obtain some useful properties from (22):

$$m = \begin{cases} \left(\frac{3(T_C - T)}{T}\right)^{1/2}, & T < T_C; \\ 0, & T > T_C. \end{cases} \quad c = -T \frac{\partial^2 f}{\partial T^2} \sim \theta(T_C - T). \quad (25)$$

The  $1/2$  exponent for magnetization  $m$  and Heaviside step function for specific heat  $c$  are typical of the mean-field Ising model.

However, in real two dimensions, the mean-field approach is not applicable and the critical phenomena are totally distinct. In fact, the 2D classical Ising model exhibits the  $1/8$  Onsager exponent for magnetization and has a logarithmic divergence in specific heat at  $T_C$  [28]:

$$m = \left(1 - (\sinh 2\beta J_1 \sinh 2\beta J_2)^{-2}\right)^{1/8}. \quad (26)$$

## 2 Single Spin Chain

In the following section, we will focus on the single spin chain with the interaction Hamiltonian:

$$H = \sum_{j=2M-1} (J_1 \sigma_j^x \sigma_{j+1}^x + J_2 \sigma_{j+1}^y \sigma_{j+2}^y), \quad m = 1, \dots, M. \quad (27)$$

Here  $2M$  is the total number of sites in the chain (see Fig. 8). And we assume the exchange constants  $J_1 < 0$ ,  $J_2 < 0$ .

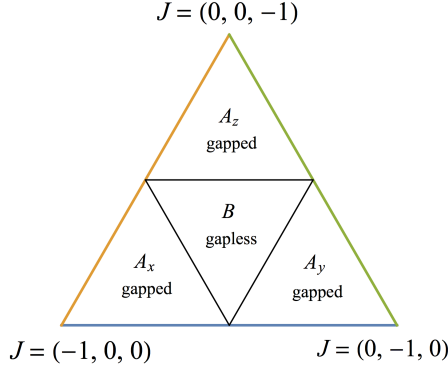


Figure 9: Phase diagram of honeycomb model where  $J = (J_1, J_2, J_3)$ .

In fact, this quantum spin chain corresponds to the bottom blue line in the phase diagram of the honeycomb lattice (see Fig. 9 and Fig. 10 (a)). The latter is solved exactly by Kitaev in a two-dimensional Majorana representation with a static  $\mathbb{Z}_2$  field [17]. From honeycomb lattices to a single chain, we can do the mapping in the following way. Firstly, it can be seen from Fig. 10 (a) and Fig. 10 (b), the honeycomb lattice is equivalent to the brick-wall lattice in an alternative representation. Then we extract a two-leg ladder into Fig. 10 (c), of which the one-dimensional limit becomes the single spin chain in Fig. 10 (d). The phase diagram in Fig. 9 consists of three

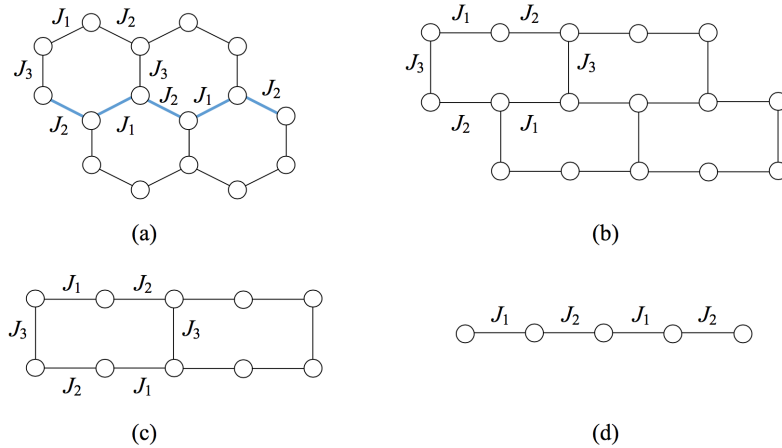


Figure 10: Mapping from a honeycomb lattice (a) to the brick-wall lattice (b), the two-leg ladder (c) and the single chain (d).

gapped spin liquid phases  $A_x, A_y$  and  $A_z$ . The gapless phase  $B$  in the middle is formed by free fermion modes. In the large  $J_3$  limit, by taking full advantage of string representations, we can extract from brick walls a single chain where the new  $A_z$  gapped phase emerges naturally as  $A_x$  and  $A_y$  phases. Fig. 11 shows three single spin chains which represent the boundaries of the phase diagram in Fig. 9. The orange and green chains correspond to  $J_2 = 0$  and  $J_1 = 0$  respectively, and they give rise to the stable  $A_z$  phase when  $J_3 \ll J_1, J_2$ . As the phase diagram is symmetric, the properties of three gapped phases are equivalent.

For the first step, we want to examine the single chain with Hamiltonian (27). As usual, we will perform Jordan-Wigner transformation to solve the quasi-particle excitation spectrum. Then we adopt Majorana chain representation to obtain the spectrum in an alternative manner. The ground state energy density gives us the information on the critical phenomena. We will see the specific heat of the quantum spin chain has a resemblance to the classical two-dimensional Ising model. Next, we introduce spin duality transformation and map the original Hamiltonian (27)

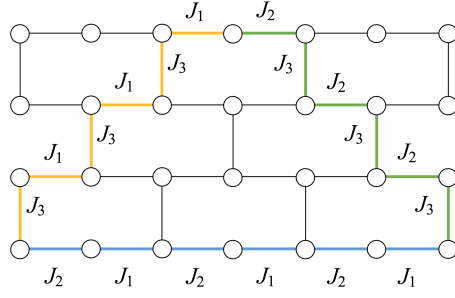


Figure 11: Construction of boundary lines for the phase diagram in honeycomb lattices.

into the transverse field Ising model (3). String order parameters show clearly the quantum phase transition between  $A_x$  and  $A_y$  spin liquid phases. In order to study their correlation function, we will go to the local Kitaev representation. In the end, we discuss the unpaired Majorana modes on each link and explore their stability in perturbation theory.

## 2.1 Eigenspectra

From now on, we change the notation of Jordan-Wigner transform into

$$\sigma_j^+ = a_j^\dagger e^{i\pi \sum_{i<j} \tilde{Q}_i}, \quad \sigma_j^- = a_j e^{i\pi \sum_{i<j} \tilde{Q}_i}, \quad \tilde{Q}_i = a_i^\dagger a_i. \quad (28)$$

In contrast with (5), we denote the spin-up state as occupied and spin-down state as empty:

$$\begin{aligned} \sigma_j^x &= (a_j^\dagger + a_j) e^{i\pi \sum_{i<j} a_i^\dagger a_i}, & \sigma_j^y &= \frac{1}{i} (a_j^\dagger - a_j) e^{i\pi \sum_{i<j} a_i^\dagger a_i}, \\ \sigma_j^z &= -i \sigma_j^x \sigma_j^y = -(a_j^\dagger + a_j)(a_j^\dagger - a_j) = 2a_j^\dagger a_j - 1 = -e^{i\pi a_i^\dagger a_i} = \begin{cases} 1, & |\uparrow\rangle; \\ -1, & |\downarrow\rangle. \end{cases} \end{aligned} \quad (29)$$

Inserting (29) into (27), we will get  $H$  in terms of fermionic operators:

$$H = \sum_{j=2m-1} (J_1(a_j^\dagger - a_j)(a_{j+1}^\dagger + a_{j+1}) - J_2(a_{j+1}^\dagger + a_{j+1})(a_{j+2}^\dagger - a_{j+2})). \quad (30)$$

To obtain the eigenspectra, we transform (30) into momentum space by

$$a_j = \frac{1}{\sqrt{2M}} \sum_k e^{ikx_j} a_k, \quad x_j = jl, \quad k = \frac{2\pi n}{l}, \quad n = -M, \dots, 0, \dots, M-1,$$

with  $l$  the lattice spacing.

$$H = \sum_k (J_1 + J_2) 2 \cos(kl) a_k^\dagger a_k + (J_2 - J_1) i \sin(kl) (a_{-k}^\dagger a_k^\dagger + a_{-k} a_k), \quad (31)$$

which can be solved in the same manner as (7). In the most general form,

$$H = \sum_k A a_k^\dagger a_k + B (a_{-k}^\dagger a_k^\dagger + a_{-k} a_k).$$

By setting  $A = -2(J_1 + J_2) \cos(kl)$ ,  $B = (J_1 - J_2) i \sin(kl)$ , we get the eigenspectra of the single spin chain immediately:

$$\epsilon_k^\pm = \pm \sqrt{\frac{A^2}{4} - B^2} = \pm \sqrt{J_1^2 + J_2^2 + 2J_1 J_2 \cos(2kl)}, \quad (32)$$

with the eigenvectors:

$$\gamma_k = u_k a_k - i v_k a_{-k}^\dagger, \quad \gamma_{-k}^\dagger = -i v_k a_k + u_k a_{-k}^\dagger,$$

where  $u_k$  and  $v_k$  satisfy

$$u_k = \cos(\theta_k/2), \quad v_k = \sin(\theta_k/2), \quad \tan(\theta_k/2) = \frac{2B}{iA} = \frac{(1-\gamma)\sin(kl)}{(1+\gamma)\cos(kl)}, \quad \gamma = \frac{J_1}{J_2}.$$

$$H = \sum_k \begin{pmatrix} \gamma_k^\dagger & \gamma_{-k} \end{pmatrix} \begin{pmatrix} \epsilon_k^+ & 0 \\ 0 & \epsilon_k^- \end{pmatrix} \begin{pmatrix} \gamma_k \\ \gamma_{-k}^\dagger \end{pmatrix} = \sum_k 2\epsilon_k^+ (\gamma_k^\dagger \gamma_k - \frac{1}{2}). \quad (33)$$

The system can be viewed as quasiparticle excitations of  $\gamma$  fermions. We denote the single-particle excitation energy as  $w(k)$ ,

$$w(k) = 2\epsilon_k^+ = 2\sqrt{J_1^2 + J_2^2 + 2J_1J_2\cos(2kl)}.$$

We easily obtain the lowest excitation energy  $\Delta = w(k)_{\min} = 2|J_1 - J_2|$ . If  $J_1 \neq J_2$ , a gap appears. The critical point is found to be  $\gamma_C = 1$  where quantum phase transition takes place.

## 2.2 Majorana chain representation

Applying Majorana operators, we introduce the notations [29]:

$$\begin{cases} c_j = i(a_j^\dagger - a_j), & d_j = a_j^\dagger + a_j, & j = 2m-1; \\ c_j = a_j^\dagger + a_j, & d_j = i(a_j^\dagger - a_j), & j = 2m. \end{cases} \quad (34)$$

Then the original Hamiltonian in (30) is transformed into

$$H = -i \sum_{j=2m-1} (J_1 c_j c_{j+1} - J_2 c_{j+1} c_{j+2}). \quad (35)$$

In total, we have  $2M$  sites with two Majoranas per site. Yet only  $c$ -type Majoranas appear in the interaction Hamiltonian once we choose a specific gauge by the definitions of  $c$ - and  $d$ -types in (34). While  $d$ -type Majoranas are all free, there is a competition to pair  $c$ -type Majoranas at a given site  $j$ . When  $J_1 \gg J_2$ , pairs  $(c_{2m-1}, c_{2m})$  are formed. There is no free  $c$ -type Majoranas. When  $J_1 \ll J_2$ , pairs  $(c_{2m}, c_{2m+1})$  are formed. We have two more free  $c$ -type Majoranas,  $c_1$  and  $c_{2M}$ .

In comparison, if we choose the notations introduced by Kitaev [25],

$$c_j = i(a_j^\dagger - a_j), \quad d_j = a_j^\dagger + a_j, \quad (36)$$

we will arrive at

$$H = -i \sum_{j=2m-1} (J_1 c_j d_{j+1} - J_2 d_{j+1} c_{j+2}). \quad (37)$$

Now, regardless of the ratio  $\gamma = J_1/J_2$ , Majoranas  $\{c_{2m}, d_{2m-1}\}$  do not appear and thus are always free. We can see the redefinition of (34) classifies these all-time free Majoranas into  $d$ -type. Then the redundant  $2M$  degrees of freedom can be removed directly in the interaction Hamiltonian.

Next, we are going to solve the eigenspectra in Majorana chain representation. For simplicity, we will use the first notation. By the Fourier transform and translational symmetry,

$$c_{k,1} = \frac{1}{\sqrt{M}} \sum_{j=2m-1} e^{-ikr_j} c_j, \quad c_{k,2} = \frac{1}{\sqrt{M}} \sum_{j=2m} e^{-ikr_j} c_j,$$

$$c_{2m-1} = \frac{1}{\sqrt{M}} \sum_k e^{ikr_{2m-1}} c_{k,1}, \quad c_{2m} = \frac{1}{\sqrt{M}} \sum_k e^{ikr_{2m}} c_{k,2},$$

where

$$r_j = jl, \quad m = 1, 2, \dots, M, \quad k = \frac{2\pi n}{2l}, \quad n = -\frac{M}{2}, \dots, 0, \dots, \frac{M}{2} - 1.$$

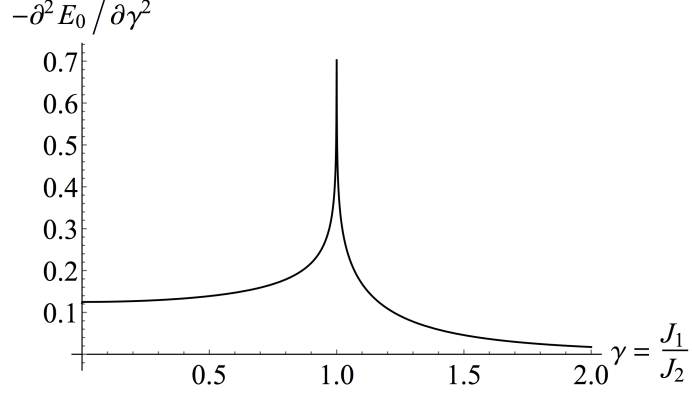


Figure 12: Second derivative of the ground state energy density. ( $J_2 = 0.5$ )

And  $c_{k,i}$  satisfies:  $c_{k,i}^\dagger = c_{-k,i}$ ,  $\{c_{k,i}, c_{k,i'}^\dagger\} = \delta_{k,k'}\delta_{i,i'}$ . Then Hamiltonian (35) becomes

$$H = \frac{1}{2} \sum_k \left( -i(J_1 e^{ikl} + J_2 e^{-ikl})c_{-k,1}c_{k,2} + i(J_1 e^{-ikl} + J_2 e^{ikl})c_{-k,2}c_{k,1} \right). \quad (38)$$

It is more convenient to work with the “double spectrum” by multiply (38) with a factor 2. To recover the “single spectrum”, we can keep only the positive eigenvalues. Now, by choosing the basis  $(c_{-k,1}, c_{-k,2})$ ,

$$H_{\text{double}} = \sum_k \begin{pmatrix} c_{-k,1} & c_{-k,2} \end{pmatrix} \begin{pmatrix} 0 & -if(k) \\ if(k)^* & 0 \end{pmatrix} \begin{pmatrix} c_{k,1} \\ c_{k,2} \end{pmatrix}, \quad f(k) = J_1 e^{ikl} + J_2 e^{-ikl}.$$

We obtain the same spectrum as (32):

$$\epsilon_k^\pm = \pm |f(k)| = \pm \sqrt{J_1^2 + J_2^2 + 2J_1 J_2 \cos(2kl)}.$$

### 2.3 Critical phenomena

We will calculate the second derivative of the ground state energy density  $E_0(\gamma)$  and check its behaviour around the critical point  $\gamma_C = 1$ . From the diagonalized Hamiltonian (33), we know

$$ME_0(\gamma) = -\frac{1}{2} \sum_{k'} w(k') = -\frac{1}{2} \int_{-2\pi(M/2-1)/l}^{2\pi M/2l} \frac{ldk'}{2\pi} w(k'),$$

$$E_0(\gamma) = -\frac{J_2(1+\gamma)}{\pi} E\left(\frac{\pi}{2}, \frac{2\sqrt{\gamma}}{1+\gamma}\right),$$

where  $E(\pi/2, s)$  is the complete elliptic integral of the second kind,

$$E(\pi/2, s) = \int_0^{\pi/2} d\theta \sqrt{1 - s^2 \sin^2 \theta}.$$

From Fig. 12, we see  $(-\partial^2 E_0/\partial\gamma^2)$  diverges logarithmically at the critical point where a gapless mode dominates.

From the mapping from 1D transverse Ising model to 2D classical Ising model, we know for the quantum model,  $(-\partial^2 E_0/\partial\gamma^2)$  corresponds to the specific heat in the classical model.

$$-\partial^2 E_0/\partial\gamma^2 \sim c = -T \frac{\partial^2 f}{\partial T^2},$$

where  $f$  is free energy per site in the classical model, which refers to the ground state energy  $E_0$  in our current quantum model. And  $\gamma$  can be viewed as a function of  $(T - T_C)/T_C$  in the exact mapping. In the mean field Ising model (25),  $c \sim \theta(T_C - T)$ . The curve of divergence in Fig. 12 shows clearly the single spin chain is not mean-field like.

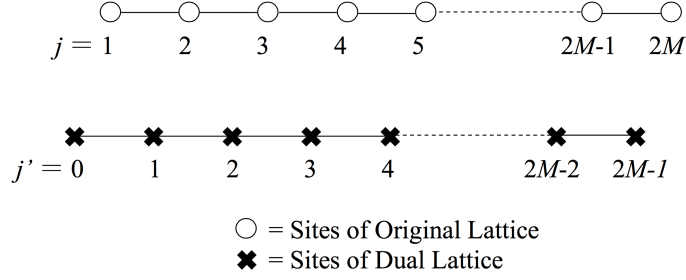


Figure 13: Dual lattices in one dimension.

## 2.4 Spin duality transformation

In fact, rather than a change of symmetry, the quantum phase transition between two superconducting phases at  $\gamma_C = 1$  involves a change of topological order of the system [29]. This point makes sense once we map the single spin chain into 1-D transverse field Ising model by spin duality transformation:

$$\tau_j^x = \prod_{k=0}^j \sigma_k^x, \quad \tau_j^y = \sigma_j^y \sigma_{j+1}^y. \quad (39)$$

While  $\tau_j^y$  represents the mutual state of  $\sigma^y$ 's at neighbouring sites  $j$  and  $j+1$ ,  $\tau_j^x$  flips all the spins to the left of site  $j$  (see Fig. 13).

For  $\sigma$  spin operators, they satisfy the algebraic relations:

$$\begin{cases} [\sigma_i^x, \sigma_j^x] = [\sigma_i^x, \sigma_j^y] = [\sigma_i^y, \sigma_j^y] = 0, & i \neq j; \\ (\sigma_j^x)^2 = (\sigma_j^y)^2 = 1, & \forall j; \\ \{\sigma_j^x, \sigma_j^y\} = 0, & \forall j. \end{cases} \quad (40)$$

On the other hand, for  $\tau$  operators, they satisfy the same relations,

$$\begin{cases} [\tau_i^x, \sigma_j^x] = [\tau_i^x, \tau_j^y] = [\tau_i^y, \tau_j^y] = 0, & i \neq j; \\ (\tau_j^x)^2 = (\tau_j^y)^2 = 1, & \forall j; \\ \{\tau_j^x, \tau_j^y\} = 0, & \forall j. \end{cases} \quad (41)$$

which implies the new variables on the dual sites are isomorphic to original ones. From (39) and (41), the inverse transformation would be

$$\sigma_j^x = \tau_{j-1}^x \tau_j^x, \quad \sigma_j^y = \prod_{k=j}^{2M} \tau_k^y. \quad (42)$$

Then the original Hamiltonian (27) can be written into the form

$$H_d = \sum_{j=1}^M (J_1 \tau_{2j-2}^x \tau_{2j}^x + J_2 \tau_{2j}^y). \quad (43)$$

In the dual space,  $H_d$  coincides with the transverse field Ising model. A similar spin duality transformation can be performed by exchanging  $x$  and  $y$  in (39) and (42):

$$H'_d = \sum_{j=1}^M (J_2 \tau_{2j-1}^y \tau_{2j+1}^y + J_1 \tau_{2j}^x). \quad (44)$$

## 2.5 String order parameter

One-dimensional Ising Model with a transverse field has been carefully examined in [30]. Following are the results closely related to our problem:

$$H_P = \sum_i (-JS_i^x S_{i+1}^x - \Gamma S_i^z), \quad J > 0, \quad \Gamma > 0, \quad (45)$$

$$\lambda = \frac{J}{\Gamma}, \quad \rho_n^x = \langle 0 | S_i^x S_{i+n}^x | 0 \rangle, \quad \lim_{n \rightarrow \infty} \rho_n^x = \begin{cases} \frac{1}{4} (1 - \lambda^{-2})^{1/4}, & \lambda > 1; \\ 0, & \lambda < 1. \end{cases} \quad (46)$$

Comparing (43) and (45), we will find

$$\gamma = J_1/J_2 = \frac{J/4}{\Gamma/2} = \frac{J}{2\Gamma} = \lambda, \quad \lim_{j \rightarrow \infty} \langle \tau_0^x \tau_{2j}^x \rangle \sim \lim_{n \rightarrow \infty} \langle 4S_i^x S_{i+n}^x \rangle = \lim_{n \rightarrow \infty} 4\rho_n^x.$$

Actually,  $\tau_0^x \tau_{2j}^x$  is the string product in the original space:

$$\hat{\Delta}_x(j) = \tau_0^x \tau_{2j}^x = \sigma_0^x \prod_{k=0}^{2j} \sigma_k^x = \prod_{k=1}^{2j} \sigma_k^x.$$

If we use the Majorana operators defined by (34),

$$\sigma_{2j-1}^x \sigma_{2j}^x = (-i)c_{2j-1}c_{2j}, \quad \hat{\Delta}_x(j) = (-i)^j \prod_{k=1}^{2j} c_k.$$

We can apply the properties (46) of transverse field Ising model directly:

$$\Delta_x = \lim_{j \rightarrow \infty} \langle \hat{\Delta}_x(j) \rangle \sim \begin{cases} (1 - (J_2/J_1)^2)^{1/4}, & |J_1| > |J_2|; \\ 0, & |J_1| < |J_2|. \end{cases} \quad (47)$$

In the same way, by comparing (44) and (45), we arrive at

$$\Delta_y = \lim_{j \rightarrow \infty} \langle \hat{\Delta}_y(j) \rangle \sim \begin{cases} 0, & |J_1| > |J_2|; \\ (1 - (J_1/J_2)^2)^{1/4}, & |J_1| < |J_2|, \end{cases} \quad (48)$$

where

$$\hat{\Delta}_y(j) = \tau_1^y \tau_{2j+1}^y = \sigma_0^y \sigma_1^y \prod_{k=0}^{2j+1} \sigma_k^y = \prod_{k=2}^{2j+1} \sigma_k^y = (+i)^j \prod_{k=2}^{2j+1} c_k.$$

Now we verify the hidden string order parameters (SOP)  $\Delta_x$  and  $\Delta_y$  which either appears nonzero or vanishes continuously at the critical point (see Fig. 14) [29]. SOPs are local in the dual space and nonlocal in the spin space. In the dual space, taking into account the change of ground state energy density in Fig. 12, we can say our original system undergoes the second-order phase transitions. What is more, the 1/4 exponents in (47) and (48) are consistent with Onsager's solution for spontaneous magnetization (26). Whereas for the mean field Ising model, the exponent appears to be 1/2 in (25).

In the original Hamiltonian (27), supposing  $J_1 \ll 0$ ,  $J_2 = 0$ , in the ground state neighbouring sites  $(2m-1, 2m)$  have the same spins due to the negative coupling constant in the interaction term  $J_1 \sigma_{2m-1}^x \sigma_{2m}^x$ . As there is no interaction between sites  $(2m, 2m+1)$ , their relative spin orientations are random (see Fig. 15 (a)). Adding a small value of  $J_2$  will not influence the ground state because the deviation of the new spin from  $x$  direction will increase the total energy of the spin chain (see Fig. 15 (b)). Consistent with (47), here we notice the topological order in  $x$  axis manifests as the nonzero spin product of coupled neighbouring pairs  $(2m-1, 2m)$ . There are an infinite number of ways to order the bonds  $(2m-1, 2m)$  along  $x$ -axis in the spin liquid ground state. At  $T = 0$ , this uncertainty produces a great amount of entropy.

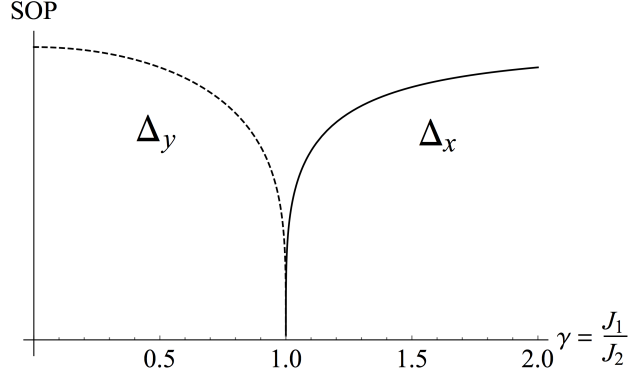


Figure 14: Nonlocal string order parameters for a single spin chain.

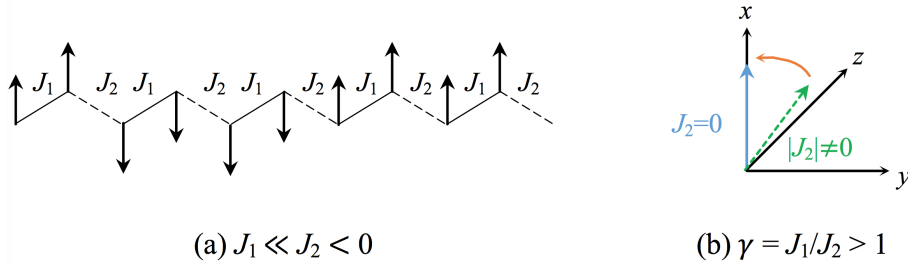


Figure 15: Spin liquid phase of the single spin chain in the ground state.

## 2.6 Local Kitaev representation

We define an algebra local in space,

$$\tilde{\sigma}_j^\alpha = ib_j^\alpha c_j, \quad \alpha = x, y, z, \quad (49)$$

such that we fulfil:

$$[\tilde{\sigma}_j^x, \tilde{\sigma}_j^y] = 2i\tilde{\sigma}_j^z, \quad [\tilde{\sigma}_j^\alpha, \tilde{\sigma}_k^{\alpha'}] = 0, \quad j \neq k. \quad (50)$$

Here the four Majorana operators satisfy anti-commutation relations:

$$c_i^\dagger = c_i, \quad (b_i^\alpha)^\dagger = b_i^\alpha, \quad \{c_i, c_j\} = \{b_i^\alpha, b_j^\alpha\} = 2\delta_{i,j}, \quad \{c_i, b_j^\alpha\} = 0.$$

Now, the original interaction Hamiltonian (27) becomes:

$$H = \sum_{j=2m-1} (J_1(ib_j^x b_{j+1}^x)(-ic_j c_{j+1}) + J_2(ib_{j+1}^y b_{j+2}^y)(-ic_{j+1} c_{j+2})), \quad (51)$$

where  $ib_j^x b_{j+1}^x$  and  $-ic_j c_{j+1}$ ,  $ib_{j+1}^y b_{j+2}^y$  and  $-ic_{j+1} c_{j+2}$  are bosonic operators with eigenvalues  $\pm 1$ . Yet only  $ib_j^x b_{j+1}^x$  and  $ib_{j+1}^y b_{j+2}^y$  commute with the total Hamiltonian. In the physical subspace  $\mathcal{L}$  of a spin-1/2 chain, each site has two degrees of freedom. We can thus restrict ourselves into common eigenspaces of  $H$ ,  $ib_j^x b_{j+1}^x$  and  $ib_{j+1}^y b_{j+2}^y$ . The ground state energy becomes

$$\langle H \rangle = \sum_{j=2m-1} (J_1(ib_j^x b_{j+1}^x)\langle -ic_j c_{j+1} \rangle + J_2(ib_{j+1}^y b_{j+2}^y)\langle -ic_{j+1} c_{j+2} \rangle).$$

Considering the case  $J_1 \ll J_2 \sim 0$ , as the spin chain is symmetric,

$$\begin{aligned} \langle -ic_j c_{j+1} \rangle &= \langle -ic_l c_{l+1} \rangle, \quad ib_j^x b_{j+1}^x = ib_l^x b_{l+1}^x, \quad \forall j, l \in \text{odd sites}, \\ \langle H \rangle &= J_1 M(ib_j^x b_{j+1}^x)\langle -ic_j c_{j+1} \rangle, \quad J_1 < 0. \end{aligned}$$

To minimise the energy, we choose to fix  $\langle -ic_j c_{j+1} \rangle > 0$ ,  $ib_j^x b_{j+1}^x = 1$  for  $j \in \text{odd sites}$ . From Fig. 15 (b), adding a small negative value of  $J_2$  will increase  $\langle H \rangle$  and we assume the pairing of neighbouring  $c$  Majoranas will always give the same sign regardless of the odd or even sites. Therefore,

$$J_2(ib_{j+1}^y b_{j+2}^y) \langle -ic_{j+1} c_{j+2} \rangle > 0, \quad J_2 < 0, \quad \langle -ic_{j+1} c_{j+2} \rangle > 0, \\ ib_{j+1}^y b_{j+2}^y = -1 < 0, \quad \forall (j+1) \in \text{even sites}.$$

In fact,  $ib_j^x b_{j+1}^x$  and  $ib_{j+1}^y b_{j+2}^y$  are operators  $\hat{u}_{jk}$  in the 2D Kitaev representation [17]. Thus we denote

$$\hat{u}_{j,j+1} = ib_j^x b_{j+1}^x, \quad \hat{u}_{j+1,j+2} = ib_{j+1}^y b_{j+2}^y, \quad j = 2m - 1,$$

with the eigenvalues

$$u_{j,j+1} = \begin{cases} +1, & \text{if } j \in \text{odd sites;} \\ -1, & \text{if } j \in \text{even sites.} \end{cases}$$

## 2.7 Correlation function

As expected, for the spin liquid, spin correlations will decay exponentially with distance in a gapped phase. We assume  $J_1 \ll J_2 \sim 0$  and examine the correlation functions  $\langle \sigma_j^x \sigma_k^x \rangle$  when  $\Delta_x \simeq 1$ .

If we fix  $j = 2m - 1$ , in the case  $k = j + 1$ ,

$$\langle H \rangle \simeq \sum_{j=2m-1} J_1 \langle \sigma_j^x \sigma_{j+1}^x \rangle \simeq M J_1 \langle \sigma_j^x \sigma_{j+1}^x \rangle, \quad \Delta_x = \left\langle \prod_{k=1}^{2j} \sigma_k^x \right\rangle \simeq (\langle \sigma_j^x \sigma_{j+1}^x \rangle)^M = 1.$$

To minimise the ground state energy  $\langle H \rangle$ , we arrive at  $\langle \sigma_j^x \sigma_{j+1}^x \rangle = 1$ . It implies  $\langle \sigma_j^x \sigma_{j+1}^x \rangle = \langle -i u_{j,j+1} c_j c_{j+1} \rangle = \langle -i c_j c_{j+1} \rangle = 1 > 0$ , consistent with our previous gauge choice.

When  $k \geq j + 2$ , the most efficient way is to start from local Kitaev representation:

$$\langle \sigma_j^x \sigma_{j+2}^x \rangle = \langle ib_j^x c_j ib_{j+2}^x c_{j+2} \rangle = \langle c_j c_{j+2} \rangle \simeq \mathcal{O} \left( e^{-\frac{|r_{j+2} - r_j|}{\xi}} \right).$$

The last approximation comes from the fact that when  $J_2 \rightarrow 0$ , there is no pairing between Majoranas on sites  $j$  and  $j + 2$ . So we can expect an exponential decay with distance and  $\xi$  is the correlation length. Accordingly,

$$k = j + 2m, \quad \langle \sigma_j^x \sigma_k^x \rangle = (-1)^{2m+2} \langle c_j c_{j+2m} \rangle \\ = \langle c_j (c_{j+2})^2 \cdots (c_{j+2m-2})^2 c_{j+2m} \rangle \simeq \langle c_j c_{j+2} \rangle \cdots \langle c_{j+2m-2} c_{j+2m} \rangle \simeq \mathcal{O} \left( e^{-\frac{|r_k - r_j|}{\xi}} \right).$$

## 2.8 Unpaired Majorana modes

In local Kitaev representation, to find free Majorana modes, we consider the case  $J_1 \ll J_2 \sim 0$ ,

$$H = \sum_{j=2m-1} -i J_1 c_j c_{j+1},$$

and introduce new  $d$ -type Majoranas in the same way as (34). We get the pairing of  $c$  Majoranas and completely free  $d$  Majoranas. Similar to the transverse Ising chain, these unpaired particles can form one qubit on each link:

$$f_j^\dagger = \frac{1}{2}(d_j + id_{j+1}), \quad f_j = \frac{1}{2}(d_j - id_{j+1}), \quad (52)$$

where

$$j = 2m - 1, \quad d_j = a_j^\dagger + a_j, \quad id_{j+1} = a_{j+1} - a_{j+1}^\dagger. \quad (53)$$

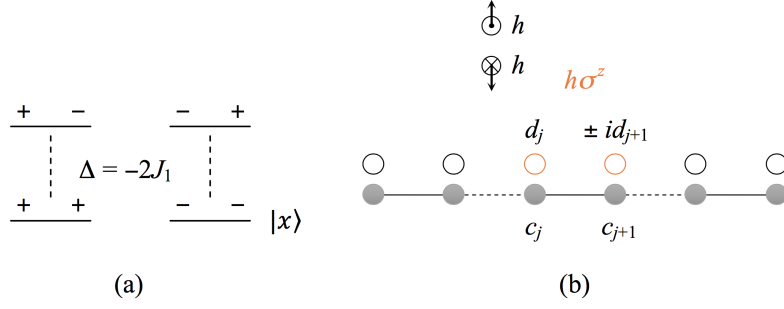


Figure 16: Ground states of a link along the single spin chain and one possible approach to exchange local qubits ( $J_2 = 0$ ).

In order to change the state of the qubit  $f^\dagger \rightarrow f$  at the  $j$ -th site, we need to find an operation to transform  $id_{j+1}$  into  $-id_{j+1}$ . We focus on a single  $J_1$ -link  $(j, j+1)$ . At  $T = 0$ , the initial system has two degenerate ground states  $|\uparrow\rangle_j \otimes |\uparrow\rangle_{j+1}$  and  $|\downarrow\rangle_j \otimes |\downarrow\rangle_{j+1}$  along  $x$ -axis, with a gap  $\Delta = -2J_1$  for first excited states (see Fig. 16 (a)). If we add a small magnetic field  $h\sigma^z$  on the local link and vary the sign of  $h$  over time, the favourable spin axis arising from this external field will change between  $|\uparrow\rangle_j \otimes |\uparrow\rangle_{j+1}$  for  $h < 0$  and  $|\downarrow\rangle_j \otimes |\downarrow\rangle_{j+1}$  for  $h > 0$ . We recall the Jordan-Wigner transformation (29)

$$\sigma_j^z = 2a_j^\dagger a_j - 1 = \begin{cases} 1, & |\uparrow\rangle_j \text{ (occupied);} \\ -1, & |\downarrow\rangle_j \text{ (empty).} \end{cases}$$

If we want to change the occupied state from  $|\uparrow\rangle_j$  to  $|\downarrow\rangle_j$ , we can redefine the fermionic operators and perform  $a_j^\dagger \longleftrightarrow a_j$ :

$$\sigma_j^z = 2a_j a_j^\dagger - 1 = 1 - 2a_j^\dagger a_j = \begin{cases} 1, & |\uparrow\rangle_j \text{ (empty);} \\ -1, & |\downarrow\rangle_j \text{ (occupied).} \end{cases}$$

It is the same for the  $(j+1)$ -th site. Taking into account (53) and (52), we arrive at

$$d_j \longleftrightarrow d_j, \quad id_{j+1} \longleftrightarrow id_{j+1}, \quad f^\dagger \longleftrightarrow f.$$

Therefore we exchange the qubit states successfully (see Fig. 16 (b)). Experimentally, applying a magnetic field along  $y$  and  $z$  axis are the same as they are both perpendicular to  $x$  direction. Meanwhile, we notice these qubits are more local than the ones in 1D quantum Ising chain. To manipulate the state of one qubit on a single link, we have to add a local magnetic field purely on two vertices.

## 2.9 Perturbation theory study

We will study the stability of  $A_x$  phase in Fig. 14 by setting  $J_1 \ll J_2 \sim 0$ .

$$H = H_0 + H',$$

$$H_0 = \sum_{j=2m-1} J_1 \sigma_j^x \sigma_{j+1}^x, \quad H' = \sum_{j=2m-1} J_2 \sigma_{j+1}^y \sigma_{j+2}^y, \quad m = 1, \dots, M.$$

As  $J_1 < 0$ , the ground state  $|GS\rangle_0$  will be the product of paralleled spins on each  $J_1$ -link. Then, we define two projection operators  $\hat{P}_0$  and  $\delta\hat{P}$ :

$$\hat{P}_0 |GS\rangle = \prod_{\{j,j+1\}} |\eta_j, \eta_{j+1}\rangle_x, \quad \delta\hat{P} = 1 - \hat{P}_0,$$

where  $\eta_j \in \{\pm 1\}$  and  $\eta_j \eta_{j+1} = 1$ . When adding  $H'$  into the full Hamiltonian,  $\hat{P}_0$  will project the new ground state onto the unperturbed  $|GS\rangle_0$ . And  $\delta\hat{P}$  will project it onto all excited states. We choose  $\begin{pmatrix} \hat{P}_0 \\ \delta\hat{P} \end{pmatrix}$  as the basis and get the eigenfunction:

$$\begin{pmatrix} P_0 H P_0 & \delta P H P_0 \\ P_0 H \delta P & \delta P H \delta P \end{pmatrix} \begin{pmatrix} \hat{P}_0 \\ \delta\hat{P} \end{pmatrix} = E \begin{pmatrix} \hat{P}_0 \\ \delta\hat{P} \end{pmatrix},$$

$$(E - P_0 H P_0)(E - \delta P H \delta P) = (P_0 H \delta P)(\delta P H P_0).$$

Then we define the effective Hamiltonian whose eigenvalues belong to  $H$  but arise from  $|GS\rangle_0$ :

$$H_{\text{eff}} = P_0 H P_0 + P_0 H \delta P \frac{1}{E - \delta P H \delta P} \delta P H P_0.$$

Setting  $E = E_0$ , for the moment we will calculate  $H_{\text{eff}}$  to the second order with higher order contributions neglected :

$$H_{\text{eff}}^{(0)} = P_0 H_0 P_0 = E_0 = M J_1, \quad H_{\text{eff}}^{(1)} = P_0 H' P_0 = 0, \quad H_{\text{eff}}^{(2)} = M \frac{J_2^2}{4J_1} \sim \hat{I}.$$

Each  $\sigma_{j+1}^y \sigma_{j+2}^y$  will flip two spins between two neighbouring  $J_1$ -links  $(j, j+1)$  and  $(j+2, j+3)$ , bringing about an increase of energy  $4|J_1|$ . However,  $H_{\text{eff}}^{(2)}$  acts as an identity operator. Therefore, for a single chain,  $A_x$  phase is stable in the presence of a small  $J_2$ . Similar arguments can be made for  $A_y$  gapped phase.

If we add Heisenberg coupling on sites  $j$  and  $j+2$ , we will find:

$$\sigma_j^x \sigma_{j+2}^x = (-ic_j c_{j+1}) id_{j+1} d_{j+2}, \quad \sigma_j^y \sigma_{j+2}^y = (-ic_{j+1} c_{j+2})(-i) d_j d_{j+1}, \quad \sigma_j^z \sigma_{j+2}^z = (-ic_j c_{j+2}) id_j d_{j+2}.$$

When  $J_1 \ll J_2 \sim 0$ , Majoranas  $c_j$  and  $c_{j+1}$  are coupled together and become massive. We have

$$\langle -ic_j c_{j+1} \rangle = 1, \quad \langle -ic_j c_{j+2} \rangle = \langle -ic_{j+1} c_{j+2} \rangle = 0,$$

$$\sigma_j^x \sigma_{j+2}^x = id_{j+1} d_{j+2}, \quad \sigma_j^y \sigma_{j+2}^y = \sigma_j^z \sigma_{j+2}^z = 0.$$

The total effect of Heisenberg coupling ( $\sigma_j^x \sigma_{j+2}^x + \sigma_j^y \sigma_{j+2}^y + \sigma_j^z \sigma_{j+2}^z$ ) will destroy free  $d$  Majoranas on the  $(j+1)$ -th and  $(j+2)$ -th sites. Therefore, to obtain spin liquid phase and free Majoranas, we should carefully tune the parameters in microscopic models and avoid the Heisenberg interaction.

### 3 Two-leg Spin Ladder

In the last section, our goal is to go above the bottom line in the phase diagram Fig. 9 and move towards the two-leg ladder in Fig. 10 (c). From Fig. 17 (c), we can write the full Hamiltonian of the ladder in the following form:

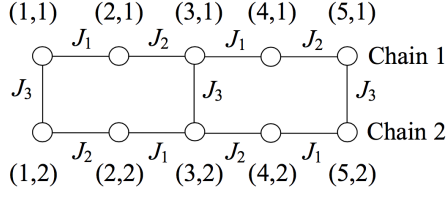
$$H = \sum_{j+l=2m} \left( J_1 \sigma_{j,l}^x \sigma_{j+1,l}^x + J_2 \sigma_{j-1,l}^y \sigma_{j,l}^y + J_3 \sigma_{j,l}^z \sigma_{j,l+1}^z \right), \quad m = 1, \dots, M. \quad (54)$$

where the coupling constants  $J_1, J_2, J_3 < 0$  and total number of sites are  $2M$ . The subscript  $(j, l)$  stands for the site at  $j$ -th row and  $l$ -th column.  $l$  can only take two values here, 1 or 2. We aim to express this Hamiltonian in terms of Majorana operators by two ways: string representation and 2D Kitaev representation. Then we will go to explore different ladders by treating the vertical links as a perturbation.

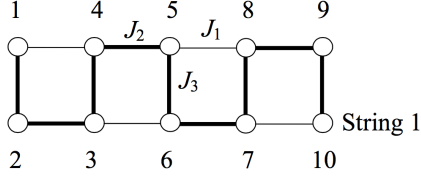
#### 3.1 Majorana picture

##### 3.1.1 String representation

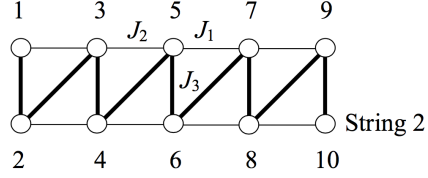
Our first approach is to perform Jordan-Wigner transformation on a one-dimensional string in the same way as the single spin chain. Fig. 17 shows two possible routes. For simplicity, we only look at the interaction terms on 5-th site along the two strings. A generalisation can be made later.



(a)



(b)



(c)

Figure 17: (a) is the two-dimensional ladder with indices  $(j, l)$  denoting  $j$ -th row and  $l$ -th column. (b) and (c) are two deformed string representations.

For String 1 in Fig. 17 (b), the interaction from  $x$  direction on the 5-th site reads

$$J_1 \sigma_5^x \sigma_8^x = J_1 (a_5^\dagger - a_5)(a_8^\dagger + a_8) e^{i\pi(a_6^\dagger a_6 + a_7^\dagger a_7)}. \quad (55)$$

As  $[a_6^\dagger a_6, J_1 \sigma_5^x \sigma_8^x] = [a_7^\dagger a_7, J_1 \sigma_5^x \sigma_8^x] = 0$ , there exists a common eigenspace in which the eigenvalues of  $a_6^\dagger a_6$  and  $a_7^\dagger a_7$  are  $c$ -numbers. We can choose a local gauge such that it minimises total ground state energy of the string. So there should be no excited particle at sites 6 and 7,  $a_6^\dagger a_6 = a_7^\dagger a_7 = 0$ . Now we turn to Fig. 17 (a) and define a set of Majorana operators:

$$c_{j,l} = \begin{cases} i(a_{j,l}^\dagger - a_{j,l}), & j+l = 2m; \\ a_{j,l}^\dagger + a_{j,l}, & j+l = 2m-1. \end{cases} \quad d_{j,l} = \begin{cases} a_{j,l}^\dagger + a_{j,l}, & j+l = 2m; \\ i(a_{j,l}^\dagger - a_{j,l}), & j+l = 2m-1. \end{cases}$$

They are Hermitian operators and satisfy anti-commutation relations:

$$c_{j,l}^\dagger = c_{j,l}, \quad d_{j,l}^\dagger = d_{j,l}, \quad \{c_{j,l}, c_{j',l'}\} = \{d_{j,l}, d_{j',l'}\} = 2\delta_{jj'}\delta_{ll'}.$$

(55) can be transformed into

$$J_1 \sigma_5^x \sigma_8^x = (-i) J_1 c_{3,1} c_{4,1}.$$

Similarly, the other two interaction terms on 5-th site become

$$\begin{aligned} J_2 \sigma_4^y \sigma_5^y &= -J_2 (a_4^\dagger + a_4)(a_5^\dagger - a_5) = i J_2 c_{2,1} c_{3,1}, \\ J_3 \sigma_5^z \sigma_6^z &= J_3 (a_5^\dagger - a_5)(a_5^\dagger + a_5)(a_6^\dagger - a_6)(a_6^\dagger + a_6) = (-i) J_3 D_{3,1} c_{3,1} c_{3,2}, \end{aligned}$$

where we introduce  $D_{j,l}$  operators on vertical bonds:  $D_{j,l} = (-i)d_{j,l}d_{j,l+1}$ . So we get the interaction Hamiltonian on the 5-th site along String 1:

$$H_{(5), \text{String 1}} = H_{(3,1), \text{String 1}} = (-i)(J_1 c_{3,1} c_{4,1} - J_2 c_{2,1} c_{3,1} + J_3 D_{3,1} c_{3,1} c_{3,2}).$$

For String 2 in Fig. 17 (c), the interaction term on the 5-th site involving  $J_3$  remains the same. Whereas for  $J_1$  and  $J_2$  parts, we should choose a different gauge:

$$\begin{aligned} J_1 \sigma_5^x \sigma_7^x &= J_1 (a_5^\dagger + a_5)(1 - 2a_5^\dagger a_5)(a_7^\dagger + a_7) e^{i\pi a_6^\dagger a_6} = (-i) J_1 c_{3,1} c_{4,1}, \\ J_2 \sigma_3^y \sigma_5^y &= -J_2 (a_3^\dagger - a_3)(1 - 2a_3^\dagger a_3)(a_5^\dagger - a_5) e^{i\pi a_4^\dagger a_4} = i J_2 c_{2,1} c_{3,1}, \end{aligned}$$

where  $a_6^\dagger a_6 = a_4^\dagger a_4 = 0$ , sites 4 and 6 are in the ground state of the string and there are no particle excitations. We see the interaction Hamiltonian including the 5-th site is the same for different routes of string:  $H_{(5), \text{String } 2} = H_{(5), \text{String } 1}$ . Further, we can generalise the results from a single site to the full ladder:

$$H_{\text{String}} = (-i) \sum_{j+l=2m} (J_1 c_{j,l} c_{j+1,l} - J_2 c_{j-1,l} c_{j,l} + J_3 D_{j,l} c_{j,l} c_{j,l+1}). \quad (56)$$

### 3.1.2 2D Kitaev representation

In fact,  $D_{j,l}$  in (56) can be fixed once we introduce Kitaev representation in two dimensions [17]. Originally it was applied onto the honeycomb lattice in Fig. 10 (a) and can be viewed as a more general form of local Kitaev representation. The spin at site  $j$  is now described by four Majorana operators  $b_j^x, b_j^y, b_j^z$  and  $c_j$ ,

$$\tilde{\sigma}_j^\alpha = i b_j^\alpha c_j, \quad \alpha = x, y, z. \quad (57)$$

They form an extended  $4N$ -dimensional Fock space  $\tilde{\mathcal{L}}$ . Whereas the physical  $2N$ -dimensional Hilbert space  $\mathcal{L}$  is defined by the operator  $D_j$ :

$$D_j = b_j^x b_j^y b_j^z c_j, \quad (58)$$

$$|\xi\rangle \in \mathcal{L}, \quad \text{iff } D_j |\xi\rangle = |\xi\rangle, \quad \forall j. \quad (59)$$

Now Pauli operators  $\sigma_j^\alpha$  acting on  $\mathcal{L}$  can be represented by new operators  $\tilde{\sigma}_j^\alpha$  on  $\tilde{\mathcal{L}}$ , which satisfy the same algebra and preserve the subspace:

$$\tilde{\sigma}_j^x \tilde{\sigma}_j^y \tilde{\sigma}_j^z = i D_j, \quad \tilde{\sigma}_j^\alpha D_i = D_i \tilde{\sigma}_j^\alpha, \quad [\tilde{\sigma}_j^\alpha, D_i] = 0.$$

where in the subspace,  $D_j$  has been viewed as identity.

We write the most general Hamiltonian of the honeycomb lattice into the form

$$\tilde{H} = \sum_{\alpha_{jk}\text{-links}} J_{\alpha_{jk}} \tilde{\sigma}_j^\alpha \tilde{\sigma}_k^\alpha, \quad \alpha = x, y, z, \quad (60)$$

where  $\alpha_{jk}$  denotes two linked interacting spins at sites  $(j, k)$  on the direction  $\alpha$  and  $J_{\alpha_{jk}}$  is the corresponding negative coupling constant. To obtain the Hamiltonian in a quadratic form, we introduce  $\hat{u}_{jk}$  operators:

$$\hat{u}_{jk} = i b_j^\alpha b_k^\alpha, \quad (61)$$

where we have already absorbed the index  $\alpha$  into the link  $(j, k)$  as the value of  $\alpha$  (direction  $x, y$  or  $z$ ) is totally determined by the choice of link  $(j, k)$  on the lattice, which means  $\alpha = \alpha_{jk}$ .  $\hat{u}_{jk}$  transforms the interaction term into

$$\tilde{\sigma}_j^\alpha \tilde{\sigma}_k^\alpha = i b_j^\alpha c_j i b_k^\alpha c_k = -i \hat{u}_{jk} c_j c_k.$$

And we notice the Hermitian operator  $\hat{u}_{jk}$  has some special properties:

$$(\hat{u}_{jk})^\dagger = \hat{u}_{jk}, \quad (\hat{u}_{jk})^2 = 1, \quad [\hat{u}_{jk}, \hat{u}_{j'k'}] = 0, \quad [\hat{u}_{jk}, c_{j'} c_{k'}] = 0, \quad (62)$$

$$[\hat{u}_{jk}, \tilde{H}] = -i \sum_{\alpha_{j'k'}\text{-links}} J_{\alpha_{j'k'}} [\hat{u}_{jk}, \hat{u}_{j'k'} c_{j'} c_{k'}] = 0. \quad (63)$$

So once we choose common eigenspaces of  $\hat{u}_{jk}$  and  $\tilde{H}$ ,  $\hat{u}_{jk}$  operators will become their eigenvalues  $u_{jk}$ , which can only be  $\pm 1$  from (62). The relative signs can be finally resolved by the application of loop operators and Lieb theorem [25]. One choice to minimise the ground state energy is

$$u_{jk} = \begin{cases} 1, & j \in \text{even sublattice;} \\ -1, & j \in \text{odd sublattice.} \end{cases} \quad (64)$$

For instance, we can denote even sublattice as  $j+l=2m$  in  $(j, l)$  notation. We write down the interaction Hamiltonian explicitly:

$$\begin{aligned} H_{\text{Loop } 1} &= (-i)(J_1 c_{1,1} c_{2,1} - J_2 c_{2,1} c_{3,1} + J_3 c_{3,1} c_{3,2} - J_1 c_{3,2} c_{2,2} + J_2 c_{2,2} c_{2,1} - J_3 c_{1,2} c_{1,1}) \\ &= (-i)(J_1(c_{1,1} c_{2,1} + c_{2,2} c_{3,2}) - J_2(c_{2,1} c_{3,1} + c_{2,1} c_{2,2}) + J_3(c_{3,1} c_{3,2} + c_{1,1} c_{1,2})). \end{aligned}$$

Comparing it with the Hamiltonian (56) within the string representation,  $D_{j,l}$  on the even sublattice is now fixed to 1. And we arrive at

$$H_{\text{Loop}} = (-i) \sum_{j+l=2m} (J_1 c_{j,l} c_{j+1,l} - J_2 c_{j-1,l} c_{j,l} + J_3 c_{j,l} c_{j,l+1}). \quad (65)$$

### 3.2 $\mathbb{Z}_2$ gauge theories and generalised ladders

In Kitaev's formalism, the fact  $u_{jk} = \pm 1$  gives rise to the  $\mathbb{Z}_2$  symmetry. And it can be generalised to a large category of 2D and 3D spin systems, where the spin interactions are link-orientation dependant and each site is connected to three different links. The two-leg ladder of our interest is a specific case.

To find gauge-invariant quantities of  $\mathbb{Z}_2$  field, we introduce loop operators:

$$W_\ell = \prod_{j \in \ell} K_{j,j+1}, \quad K_{j,j+1} = \sigma_j^\alpha \sigma_{j+1}^\alpha, \quad \alpha = x, y, z, \quad (66)$$

where  $j$  labels the sites along the loop  $\ell$  and  $\alpha$  denotes the direction of spin interactions on each link.

Now suppose the loop has even-length  $2n$ , in the 2D Kitaev representation,

$$\begin{aligned} K_{j,j+1} &= (ib_j^\alpha c_j)(ib_{j+1}^\alpha c_{j+1}) = -i \hat{u}_{j,j+1} c_j c_{j+1}, \\ W_\ell &= K_{1,2} K_{2,3} \cdots K_{2n,1} = (-1)^n \hat{u}_{1,2} \hat{u}_{2,3} \cdots \hat{u}_{2n,1}. \end{aligned}$$

Hence,

$$[W_\ell, H] = 0, \quad W_\ell = (-1)^n u_{1,2} u_{2,3} \cdots u_{2n,1} = \pm 1. \quad (67)$$

There exist macroscopic number of conserved quantities associated to the loops. Considering  $u_{j,k} = -u_{k,j}$ , we can rearrange (67) into the product of  $u_{\text{even,odd}}$ :

$$W_\ell = u_{2,1} u_{2,3} \cdots u_{2n,2n-1} u_{2n,1}. \quad (68)$$

According to Lieb's theorem [31], in the ground state

$$W_\ell = \begin{cases} 1, & 2n \pmod{4} = 2; \\ -1, & 2n \pmod{4} = 0, \end{cases} \quad (69)$$

where 1 and  $-1$  refer to the 0 and  $\pi$  flux configurations. Combining (68) and (69), we can choose appropriate gauges for  $u_{j,k}$  in different lattices. It is easy to check for the honeycomb lattice  $2n=6$ , Kitaev's choice (64) satisfies the right ground state flux configuration without any vortices  $W_\ell = 1$ .

Now we can apply the same principle to various two-leg ladder systems. Mainly, we consider three types of plaquettes with the loop length 4, 6 and 8 respectively (see Fig. 18). Interactions on vertical links are all from  $z$ -axis. We label the signs of  $u_{j,j+1}$  along each loop. While Fig. 18 (a) mapped from the honeycomb lattice has a 0 flux, Fig. 18 (a) and Fig. 18 (c) share the  $\pi$  flux in their plaquettes. These gauge choices are not unique, but different gauges will give the same spectra once we perform gauge transformations.

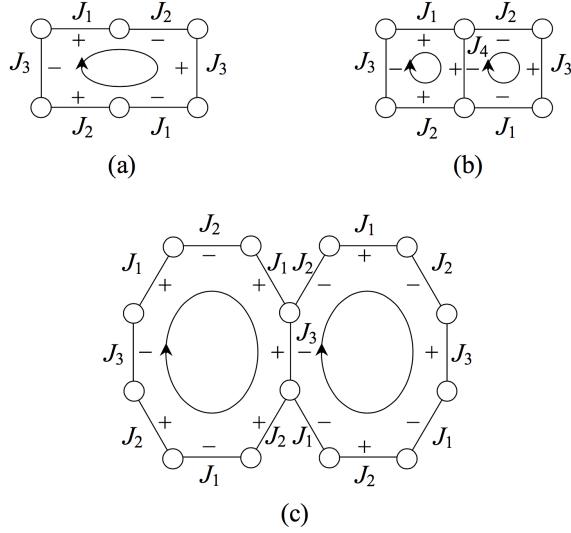


Figure 18: Gauges for  $u_{j,j+1}$  along the loops in different shapes of plaquettes.

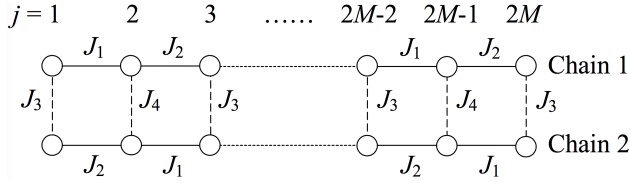


Figure 19: Ladder with weak vertical bonds.

### 3.3 Phase diagram with $J_4$

We consider the ladder with  $J_4$ -links in Fig. 19. Our strategy is to start from two single spin chains, solve them independently and add extra interaction terms as a perturbation. In such a way, two chains are connected into a ladder by weak vertical bonds.

#### 3.3.1 Free fermion model

Firstly, we take a glance at a free fermion model in Fig. 20 to illustrate this idea:

$$H_1 = -t_{\parallel} \sum_j (a_{j,1}^{\dagger} a_{j+1,1} + \text{h.c.}), \quad H_2 = -t_{\parallel} \sum_j (a_{j,2}^{\dagger} a_{j+1,2} + \text{h.c.}),$$

$$H_{\perp} = -t_{\perp} \sum_j (a_{j,1}^{\dagger} a_{j,2} + \text{h.c.}).$$

Here  $H_1$  and  $H_2$  are hopping terms for two independent spin chains and  $H_{\perp}$  comes from the small vertical interaction ( $t_{\parallel}, t_{\perp} > 0$ ).

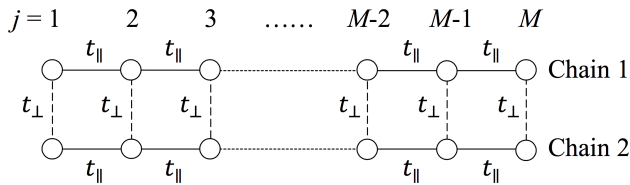


Figure 20: Two-leg free fermion ladder.

By Fourier transform into the momentum space,

$$a_{j,1} = \frac{1}{\sqrt{M}} \sum_k e^{ikr_j} a_{k,1}, \quad a_{j,2} = \frac{1}{\sqrt{M}} \sum_k e^{ikr_j} a_{k,2},$$

$$k = \frac{2\pi m}{l}, \quad m = -\frac{M}{2}, \dots, 0, \dots, \frac{M}{2} - 1,$$

where  $M$  is the number of sites for each chain and  $l$  is the lattice spacing, we get the full Hamiltonian in the form

$$H = H_1 + H_2 + H_\perp$$

$$= \sum_k (-2t_\parallel \cos kl) (a_{k,1}^\dagger a_{k,1} + a_{k,2}^\dagger a_{k,2}) - t_\perp (a_{k,1}^\dagger a_{k,2} + a_{k,2}^\dagger a_{k,1}). \quad (70)$$

We see clearly the existence of  $t_\perp$  makes the hopping between two chains possible, which gives rise to the bonding ( $B$ ) and anti-bonding ( $A$ ) eigenstates:

$$\gamma_k = \frac{1}{\sqrt{2}} (a_{k,1} + a_{k,2}), \quad \eta_k = \frac{1}{\sqrt{2}} (a_{k,1} - a_{k,2}),$$

with the energy spectra:

$$H = \sum_k (\epsilon_k^B \gamma_k^\dagger \gamma_k + \epsilon_k^A \eta_k^\dagger \eta_k), \quad \epsilon_k^B = -2t_\parallel \cos kl - t_\perp, \quad \epsilon_k^A = -2t_\parallel \cos kl + t_\perp.$$

When  $t_\perp = 0$ , two bands overlap (see Fig. 21 (a)). With zero chemical potential  $k_F$  are fixed to  $\pi/2l$ , so both of the bands are half-filling. In Fig. 21 (b), by contrast small  $t_\perp$  will open a gap  $\Delta = 2t_\perp$  and leave the fermi level cross two bands. When  $t_\perp$  gets larger than  $t_\parallel$  in Fig. 21 (c), however, the degeneracy is completely removed and the bonding state becomes the single ground state.

### 3.3.2 $J_4$ ladder

In the same way, for the ladder in Fig. 19 we decompose Hamiltonian (65) into three parts : Chain 1, Chain 2 and the vertical bonds,

$$H_1 = (-i) \sum_{j=2m-1} (J_1 c_j c_{j+1} - J_2 c_{j+1} c_{j+2}), \quad H_2 = (-i) \sum_{j=2m-1} (-J_2 c'_j c'_{j+1} + J_1 c'_{j+1} c'_{j+2}),$$

$$H_\perp = (-i) \sum_{j=2m-1} (J_3 c_j c'_j + J_4 c_{j+1} c'_{j+1}).$$

Here we only select odd  $j$  and  $l$  denotes the chain number. And the relative signs in front of coupling constants are determined from loops in square plaquettes (see Fig. 18 (b)).

We perform the Fourier transform of Majorana operators on each chain independently:

$$c_{2m-1} = \frac{1}{\sqrt{M}} \sum_k e^{ikr_{2m-1}} c_{k,1}, \quad c_{2m} = \frac{1}{\sqrt{M}} \sum_k e^{ikr_{2m}} c_{k,2},$$

$$c'_{2m-1} = \frac{1}{\sqrt{M}} \sum_k e^{ikr_{2m-1}} c'_{k,1}, \quad c'_{2m} = \frac{1}{\sqrt{M}} \sum_k e^{ikr_{2m}} c'_{k,2},$$

where

$$k = \frac{2\pi n}{2l}, \quad n = -\frac{M}{2}, \dots, \frac{M}{2} - 1.$$

The unperturbed Hamiltonians become

$$H_1 = \sum_k \begin{pmatrix} c_{-k,1} & c_{-k,2} \end{pmatrix} \begin{pmatrix} 0 & -if_1(k) \\ if_1^*(k) & 0 \end{pmatrix} \begin{pmatrix} c_{k,1} \\ c_{k,2} \end{pmatrix},$$

$$H_2 = \sum_k \begin{pmatrix} c'_{-k,1} & c'_{-k,2} \end{pmatrix} \begin{pmatrix} 0 & -if_2(k) \\ if_2^*(k) & 0 \end{pmatrix} \begin{pmatrix} c'_{k,1} \\ c'_{k,2} \end{pmatrix},$$

$$f_1(k) = J_1 e^{-ikl} + J_2 e^{ikl}, \quad f_2(k) = -J_1 e^{ikl} - J_2 e^{-ikl} = -f_1^*(k).$$

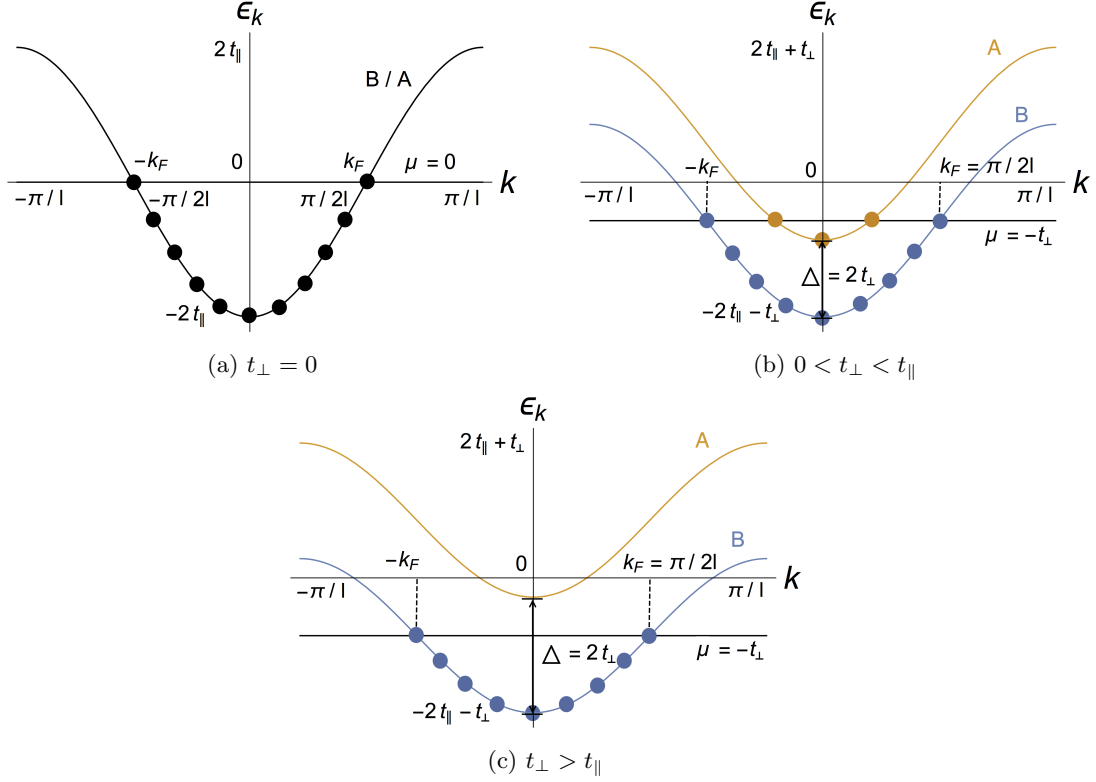


Figure 21: Band structures of free fermion model with different strengths of vertical couplings.  $B$  denotes the bonding band and  $A$  the antibonding band.

And the perturbation term will be

$$H_{\perp} = (-i) \sum_k (J_3(c_{-k,1}c'_{k,1} - c'_{-k,1}c_{k,1}) + J_4(c_{-k,2}c'_{k,2} - c'_{-k,2}c_{k,2})).$$

We obtain the energy spectrum by diagonalizing the full Hamiltonian:

$$H = \sum_k \begin{pmatrix} c_{-k,1} & c_{-k,2} & c'_{-k,1} & c'_{-k,2} \end{pmatrix} \begin{pmatrix} 0 & -if_1 & -iJ_3 & 0 \\ if_1^* & 0 & 0 & -iJ_4 \\ iJ_3 & 0 & 0 & -if_2 \\ 0 & iJ_4 & if_2^* & 0 \end{pmatrix} \begin{pmatrix} c_{k,1} \\ c_{k,2} \\ c'_{k,1} \\ c'_{k,2} \end{pmatrix},$$

$$\epsilon_i^2(k) = C + \frac{1}{2}(J_3^2 + J_4^2) \pm \frac{1}{2} \left( (J_3^2 - J_4^2)^2 + 4C(J_3^2 + J_4^2) + 4DJ_3J_4 \right)^{1/2}, \quad i = 1, 2, 3, 4, \quad (71)$$

with

$$C = |f_1|^2 = |f_2|^2 = J_+^2 \cos^2(kl) + J_-^2 \sin^2(kl), \quad J_{\pm} = J_1 \pm J_2,$$

$$D = f_1 f_2^* + f_1^* f_2 = -4J_1 J_2 - 2(J_1^2 + J_2^2) \cos(2kl).$$

We see two identical bands split into four branches. And the energy spectrum is invariant under the spontaneous transformation  $J_1 \rightarrow -J_1, J_2 \rightarrow -J_2, J_3 \rightarrow -J_3$ . Only the ground state will change from ferromagnetic to antiferromagnetic configurations on each link.

In comparison with the free fermion model,

$$J_3 \sim t_{\perp}.$$

We can expect when  $J_3 = t_{\perp} = 0$ , four branches of bands will overlap with each other and we get band structure like Fig. 21 (a). When  $|J_3| \gg |J_1, J_2|$ , in the ground state we are left with a single band and the system is again in the  $A_z$  phase like the 1D chain (see Fig. 21 (c)). Yet what happens in between becomes much more complicated. There are crossovers of different bands in Fig. 21 (b). We will discuss one case for  $J_3 = J_4$ , later in Sec. 3.3.4.

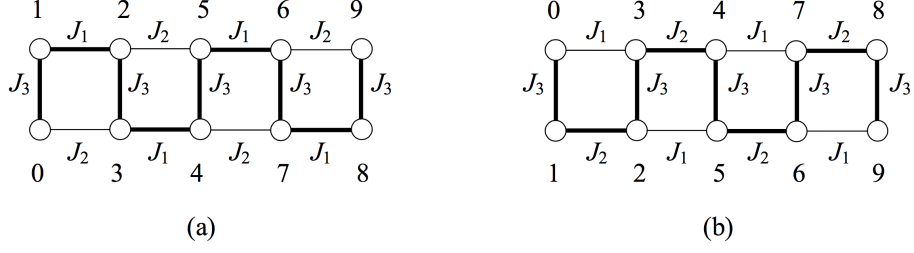


Figure 22: Two deformed string representations for  $J_4 = J_3$ .

### 3.3.3 $J_4 = 0$

Without  $J_4$ -links, we return to the ladder limit of honeycomb lattices in Fig. 17 (a). Constructing a bigger loop in rectangles will not change the relative sign before  $J_1, J_2, J_3$ . Then we can set  $J_4 = 0$  directly in (71):

$$\epsilon_i^2(k) = C + \frac{1}{2}J_3^2 \pm \frac{1}{2}(J_3^4 + 4CJ_3^2)^{1/2}, \quad i = 1, 2, 3, 4.$$

### 3.3.4 $J_4 = J_3$

If  $J_4$  coincides with  $J_3$ , the energy spectrum will become

$$\epsilon_k = \pm \sqrt{(J_3 \pm J_- \sin(kl))^2 + J_+^2 \cos^2(kl)}.$$

The quasiparticle excitation gap disappears at  $J_3 = \pm J_-$ . Like the single spin chain, it indicates quantum phase transitions. In fact, in the ground state, the ladder now can be mapped into  $XY$  model by similar spin duality transformation [29]. And there is long range order along  $x$  and  $y$  directions in different cases.

Nonzero spin order parameter  $\Delta_x$  can be found by choosing string representation in Fig. 22 (a). The Hamiltonian has the following form:

$$H = \sum_{j=1}^{2M} (J_1 \sigma_{2j-1}^x \sigma_{2j}^x + J_3 \sigma_{2j-2}^z \sigma_{2j-1}^z + J_2 \sigma_{2j-2}^y \sigma_{2j+1}^y).$$

Further, we perform the spin duality transformation along the string in  $x$  and  $z$  directions:

$$\tau_j^z = \sigma_j^z \sigma_{j+1}^z, \quad \tau_j^x = \prod_{k=0}^j \sigma_k^x, \quad \sigma_j^z = \prod_{k=j}^{4M} \tau_k^z, \quad \sigma_j^x = \tau_{j-1}^x \tau_j^x. \quad (72)$$

In dual space, we obtain the new Hamiltonian:

$$H_D = \sum_{j=1}^{2M} (J_1 \tau_{2j-2}^x \tau_{2j}^x + J_2 W_2 \tau_{2j-2}^y \tau_{2j}^y + J_3 \tau_{2j-2}^z), \quad W_2 = \tau_{2j-3}^x \tau_{2j-1}^z \tau_{2j+1}^x. \quad (73)$$

Here the loop operator  $W_{2j}$  is a good quantum number and appears to be  $(-1)$  in the ground state, exhibiting a  $\pi$ -flux phase [31]. Now we arrive at the  $XY$  model:

$$H_{XY} = \sum_{j=1}^N ((1 + \gamma)JS_j^x S_{j+1}^x + (1 - \gamma)JS_j^y s_{j+1}^y - h\mu S_j^z),$$

$$(1 + \gamma)J = 4J_1, \quad (1 - \gamma)J = -4J_2, \quad 2J_3 = -h\mu, \quad l' = 2l, \quad N = 2M.$$

From [32], it can be shown that for  $J = 2J_- > 0, \gamma = J_+/J_- < -1$ ,

$$\lim_{R \rightarrow \infty} \rho_{xx}(R) = \lim_{R \rightarrow \infty} \langle S_j^x S_{j+R}^x \rangle = \begin{cases} \frac{1}{2(1-\gamma)} \left( \gamma^2 \left( 1 - \left( \frac{h\mu}{J} \right)^2 \right) \right)^{1/4}, & |h\mu| < J; \\ 0, & \text{otherwise.} \end{cases} \quad (74)$$

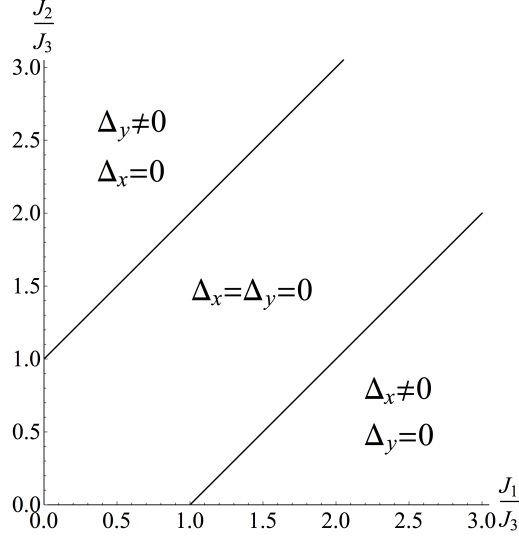


Figure 23: Phase diagram of the two-leg ladder ( $J_4 = J_3$ ).

In real space, it implies

$$\begin{aligned} \Delta_x &= \lim_{j \rightarrow \infty} \langle \prod_{k=0}^{2j} \sigma_k^x \rangle = \lim_{j \rightarrow \infty} \langle \tau_0^x \tau_{2j}^x \rangle = \lim_{R \rightarrow \infty} 4\rho_{xx}(R) \\ &= \begin{cases} \frac{2|J_+/J_-|^{1/2}}{(1+|J_+/J_-|)} \left(1 - (J_3/J_-)^2\right)^{1/4}, & |J_3| < J_-; \\ 0, & \text{otherwise.} \end{cases} \end{aligned} \quad (75)$$

For  $\Delta_y$ , we can choose a different string route. Fig. 22 (b) shows the simplest one. Making spontaneous exchanges of  $x$  and  $y$ ,  $J_1$  and  $J_2$  in (72)  $\sim$  (75) gives

$$\Delta_y = \lim_{j \rightarrow \infty} \langle \prod_{k=0}^{2j} \sigma_k^y \rangle = \lim_{j \rightarrow \infty} \langle \tau_0^y \tau_{2j}^y \rangle = \begin{cases} \frac{2|J_+/J_-|^{1/2}}{(1+|J_+/J_-|)} \left(1 - (J_3/J_-)^2\right)^{1/4}, & |J_3| < -J_-; \\ 0, & \text{otherwise.} \end{cases}$$

We recover the phase diagram of the ladder in [29] (see Fig. 23).

## Conclusion

From the transverse Ising model to quantum single spin chain and two-leg ladders, we have studied various low-dimensional microscopic models with  $1/2$  spin and built their connections with the BCS Hamiltonian. It can be seen that Majorana particle originates both from superconductivity and magnetism.

In the transverse Ising model, we apply Jordan-Wigner transformation to obtain the BCS ground state and find the critical temperature  $g_C = 1$  where quantum phase transition takes place. In 1D Kitaev representation, free Majorana bound states are proved to exist at each end of the Ising chain. They form two states of qubits and can be exchanged in the presence of small magnetic field at zero temperature. For the single spin chain, under spin duality transformation the original Hamiltonian is mapped onto the transverse field Ising model in the dual space. String order parameter enables us to distinguish two spin liquid phases  $A_x$  and  $A_y$  for  $\gamma > 1$  and  $\gamma < 1$ . By studying correlation function with the help of local Kitaev representation, we see the long range order is clearly absent from spin liquid phases. These exotic quantum phases are quite stable and may preserve disorder to very low temperatures. In addition, two free Majoranas are found on each link along the chain and we point out their fragility under Heisenberg couplings, a key disadvantage

for real quantum materials. In the end, after a comparison of different Majorana pictures in two dimensions, we deep into  $\mathbb{Z}_2$  gauge theories and fix the gauges for generalised ladders based on 2D Kitaev representation and Lieb's theorem. As an application, the spectrum and phase diagram of a two-leg spin-1/2 ladder with  $J_4$  links are solved.

In contrast to the spin-1/2 Heisenberg chains where there is a power-law decay in the spin correlation function, the spin liquid phase obtained in our model exhibits a much faster exponential decay.

And it should also be noticed there is remarkable distinction between integer and half-integer spins [33]. The Hamiltonian for the antiferromagnetic (AF) Heisenberg spin chain reads:

$$H = J \sum_i \vec{S}_i \cdot \vec{S}_{i+1}, \quad (76)$$

where  $J > 0$ . In Haldane's conjecture [24], the action describing the spin- $S$  AF Heisenberg chain at low energies has the following form:

$$S_{\text{effective}} = \frac{v}{2g} \int d\tau dx \left( \frac{1}{v^2} (\partial_\tau \vec{n})^2 + (\partial_x \vec{n})^2 \right) + i2\pi S \mathcal{Q}(\vec{n}), \quad (77)$$

$$\mathcal{Q}(\vec{n}) = \int d\tau dx \vec{n} \cdot (\partial_\tau \vec{n} \wedge \partial_x \vec{n}) / 4\pi,$$

where  $v = 2JS, g = 2/S$ .  $\vec{n}$  is the order parameter of the Néel collinear state and  $\mathcal{Q}(\vec{n})$  measures the number of times  $\vec{n}$  covers the surface of unit sphere  $S^2$ . Haldane found for integer spins, the topological term  $2\pi S \mathcal{Q}(\vec{n})$  can be neglected and then (77) is reduced to the 2D  $O(1)$  nonlinear sigma model with a finite energy spin gap and non-trivial edge excitations. Five years later in 1988, the existence of the Haldane gap was validated in  $\text{Ni}(\text{C}_2\text{H}_8\text{N}_2)_2\text{NO}_2(\text{ClO}_4)$  (NENP) compounds [34]. If we add a frustration term into the Hamiltonian (76):

$$H_\beta = J \sum_i \left( \vec{S}_i \cdot \vec{S}_{i+1} + \beta \left( \vec{S}_i \cdot \vec{S}_{i+1} \right)^2 \right),$$

when  $S = 1, \beta = 1/3$ , it is mapped onto the AKLT model whose ground state can be exactly solved while major characteristics of the Haldane spin liquid phase are maintained.

For half-integer spins, on the contrary,  $2\pi S \mathcal{Q}(\vec{n})$  gives a phase factor  $(-1)^{\mathcal{Q}}$  to the path integral in the effective action (77). Quantum interference occurs between topologically distinct paths. Therefore, we can expect unusual magnetism and unique quantum phase transitions for our spin-1/2 models.

In the future, on the theoretical side we can extend the spin-1/2 ladder models to two-dimensional and three-dimensional lattices. In higher dimensions, combined with projective time-reversal and inversion symmetries for a given lattice, Majorana fermions and the  $\mathbb{Z}_2$  gauge field introduced by A. Kitaev are still essential for the classification of exotic spin liquid phases [35]. On the practical side, for the potential applications in quantum computing, the braiding of Majoranas is also intriguing. Surface mini-codes have successfully been built in superconducting quantum circuits [36], which involve only nearest-neighbour coupling and rapidly cycled entangling gates. Large-scale, fault-tolerant and multi-qubit Majorana-based quantum codes will continue to pave the way for quantum computation in coming times.

## References

- [1] J Schechter and José WF Valle. Neutrino masses in  $SU(2) \otimes U(1)$  theories. *Physical Review D*, 22(9):2227, 1980.
- [2] Steven R Elliott and Marcel Franz. Colloquium: Majorana fermions in nuclear, particle, and solid-state physics. *Reviews of Modern Physics*, 87(1):137, 2015.
- [3] Werner Rodejohann. Neutrino-less double beta decay and particle physics. *International Journal of Modern Physics E*, 20(09):1833–1930, 2011.
- [4] Vladimir Tello, Miha Nemevšek, Fabrizio Nesti, Goran Senjanović, and Francesco Vissani. Left-right symmetry: From the LHC to neutrinoless double beta decay. *Physical review letters*, 106(15):151801, 2011.
- [5] Nicholas Read and Dmitry Green. Paired states of fermions in two dimensions with breaking of parity and time-reversal symmetries and the fractional quantum hall effect. *Physical Review B*, 61(15):10267, 2000.
- [6] A Yu Kitaev. Unpaired Majorana fermions in quantum wires. *Physics-Uspekhi*, 44(10S):131, 2001.
- [7] Liang Fu and Charles L Kane. Superconducting proximity effect and majorana fermions at the surface of a topological insulator. *Physical review letters*, 100(9):096407, 2008.
- [8] Pouyan Ghaemi and Frank Wilczek. Near-zero modes in superconducting graphene. *Physica Scripta*, 2012(T146):014019, 2012.
- [9] Doron L Bergman and Karyn Le Hur. Near-zero modes in condensate phases of the dirac theory on the honeycomb lattice. *Physical Review B*, 79(18):184520, 2009.
- [10] Yuval Oreg, Gil Refael, and Felix von Oppen. Helical liquids and majorana bound states in quantum wires. *Physical review letters*, 105(17):177002, 2010.
- [11] Roman M Lutchyn, Jay D Sau, and S Das Sarma. Majorana fermions and a topological phase transition in semiconductor-superconductor heterostructures. *Physical review letters*, 105(7):077001, 2010.
- [12] Vincent Mourik, Kun Zuo, Sergey M Frolov, SR Plissard, EPAM Bakkers, and LP Kouwenhoven. Signatures of Majorana fermions in hybrid superconductor-semiconductor nanowire devices. *Science*, 336(6084):1003–1007, 2012.
- [13] Jie Liu, Andrew C Potter, Kam Tuen Law, and Patrick A Lee. Zero-bias peaks in the tunneling conductance of spin-orbit-coupled superconducting wires with and without majorana end-states. *Physical review letters*, 109(26):267002, 2012.
- [14] Stevan Nadj-Perge, Ilya K Drozdov, Jian Li, Hua Chen, Sangjun Jeon, Jungpil Seo, Allan H MacDonald, B Andrei Bernevig, and Ali Yazdani. Observation of Majorana fermions in ferromagnetic atomic chains on a superconductor. *Science*, 346(6209):602–607, 2014.
- [15] John Bardeen, Leon N Cooper, and John Robert Schrieffer. Theory of superconductivity. *Physical Review*, 108(5):1175, 1957.
- [16] V Gurarie and L Radzihovsky. Zero modes of two-dimensional chiral p-wave superconductors. *Physical Review B*, 75(21):212509, 2007.
- [17] Alexei Kitaev. Anyons in an exactly solved model and beyond. *Annals of Physics*, 321(1):2–111, 2006.

- [18] Jeffrey G Rau, Eric Kin-Ho Lee, and Hae-Young Kee. Spin-orbit physics giving rise to novel phases in correlated systems: Iridates and related materials. *arXiv preprint arXiv:1507.06323*, 2015.
- [19] A Banerjee, CA Bridges, J-Q Yan, AA Aczel, L Li, MB Stone, GE Granroth, MD Lumsden, Y Yiu, J Knolle, S Bhattacharjee, DL Kovrizhin, R Moessner, DA Tennant, DG Mandrus, and SE Nagler. Proximate Kitaev quantum spin liquid behaviour in a honeycomb magnet. *Nature materials*, 2016.
- [20] L-M Duan, E Demler, and MD Lukin. Controlling spin exchange interactions of ultracold atoms in optical lattices. *Physical review letters*, 91(9):090402, 2003.
- [21] P Jordan and Eugene P Wigner. About the pauli exclusion principle. *Z. Phys*, 47(631):14–75, 1928.
- [22] Paul AM Dirac. The fundamental equations of quantum mechanics. In *Proceedings of the Royal Society of London A: Mathematical, Physical and Engineering Sciences*, volume 109, pages 642–653. The Royal Society, 1925.
- [23] T Holstein and H Primakoff. Field dependence of the intrinsic domain magnetization of a ferromagnet. *Physical Review*, 58(12):1098, 1940.
- [24] F Duncan M Haldane. Continuum dynamics of the 1-D Heisenberg antiferromagnet: identification with the O(3) nonlinear sigma model. *Physics Letters A*, 93(9):464–468, 1983.
- [25] Alexei Kitaev and Chris Laumann. Topological phases and quantum computation. *arXiv preprint arXiv:0904.2771*, 2009.
- [26] LS Levitov, TP Orlando, JB Majer, and JE Mooij. Quantum spin chains and majorana states in arrays of coupled qubits. *arXiv preprint cond-mat/0108266*, 2001.
- [27] Subir Sachdev. *Quantum phase transitions*. Cambridge University Press, 2011.
- [28] Kerson Huang. *Statistical mechanics*. New York - London, 1963.
- [29] Xiao-Yong Feng, Guang-Ming Zhang, and Tao Xiang. Topological characterization of quantum phase transitions in a spin-1/2 model. *Physical review letters*, 98(8):087204, 2007.
- [30] Pierre Pfeuty. The one-dimensional ising model with a transverse field. *ANNALS of Physics*, 57(1):79–90, 1970.
- [31] Elliott H Lieb. Flux phase of the half-filled band. In *Condensed Matter Physics and Exactly Soluble Models*, pages 79–82. Springer, 2004.
- [32] Eytan Barouch and Barry M McCoy. Statistical mechanics of the x y model. ii. spin-correlation functions. *Physical Review A*, 3(2):786, 1971.
- [33] Hung T Diep. *Frustrated spin systems*. World Scientific, 2013.
- [34] JP Renard, LP Regnault, and M Verdaguer. Experimental evidences for an Haldane gap in quasi one-dimensional antiferromagnets. *Le Journal de Physique Colloques*, 49(C8):C8–1425, 1988.
- [35] Kevin O’Brien, Maria Hermanns, and Simon Trebst. Classification of gapless  $Z_2$  spin liquids in three-dimensional kitaev models. *Physical Review B*, 93(8):085101, 2016.
- [36] R Barends, J Kelly, A Megrant, A Veitia, D Sank, E Jeffrey, TC White, J Mutus, AG Fowler, B Campbell, et al. Superconducting quantum circuits at the surface code threshold for fault tolerance. *Nature*, 508(7497):500–503, 2014.